

# A Tsunami Forecast Model for Morehead City, North Carolina

Hongqiang Zhou<sup>1,2</sup>

1. NOAA Center for Tsunami Research, Pacific Marine Environmental Laboratory, Seattle, WA
2. Joint Institute for the Study of the Atmosphere and Ocean, Seattle, WA

## Contents

<b>Abstract</b>	<b>5</b>
<b>1 Background and Objectives</b>	<b>6</b>
<b>2 Forecast Methodology</b>	<b>7</b>
<b>3 Model Development</b>	<b>8</b>
3.1 Forecast area . . . . .	8
3.2 Digital elevation models . . . . .	8
3.3 Grid setup . . . . .	9
<b>4 Model Testing</b>	<b>10</b>
4.1 Accuracy . . . . .	10
4.2 Stability . . . . .	11
<b>5 Conclusions</b>	<b>11</b>
<b>Acknowledgement</b>	<b>12</b>
<b>References</b>	<b>13</b>
<b>Figures</b>	<b>15</b>
<b>A Model *.in files for Morehead City, North Carolina</b>	<b>27</b>
A.1 Reference model *.in file . . . . .	27
A.2 Forecast model *.in file . . . . .	27
<b>B Propagation Database:     Atlantic Ocean Unit Sources</b>	<b>28</b>
<b>C Forecast Model Testing</b>	<b>36</b>
C.1 Purpose . . . . .	36
C.2 Testing procedure . . . . .	36
C.3 Results . . . . .	37

## List of Figures

1	Morehead City, North Carolina, and the surrounding vicinity (courtesy of Google Maps). . . . .	16
2	Grid extents of the Morehead City forecast model: (a) grid extents, (b) bathymetry and topography of the C grid. The triangles in the C grid denote the tide stations near Spooners Creek and Beaufort Harbor. . . . .	17
3	Grid extents of the Morehead City reference model: (a) grid extents, (b) bathymetry and topography of the C grid. The triangles in (b) denote the tide stations at Spooners Creek and Beaufort Harbor. . . . .	18
4	Epicenters of triggering earthquakes in synthetic mega-tsunami scenarios employed to test the Morehead City, North Carolina forecast and reference models. Location of Morehead City is indicated as a star in the map. . . . .	19
5	Model results for mega-tsunami scenario ATSZ 38-47. The upper panels show the distribution of maximum water surface elevations. The lower panels show the time series of water surface elevations at tide stations. . . . .	20
6	Model results for scenario ATSZ 48-57. The upper panels show the distribution of maximum water surface elevations. The lower panels show the time series of water surface elevations at tide stations. . . . .	20
7	Model results for mega-tsunami scenario ATSZ 58-67. The upper panels show the distribution of maximum water surface elevations. The lower panels show the time series of water surface elevations at tide stations. . . . .	21
8	Model results for mega-tsunami scenario ATSZ 68-77. The upper panels show the distribution of maximum water surface elevations. The lower panels show the time series of water surface elevations at tide stations. . . . .	21
9	Model results for mega-tsunami scenario ATSZ 82-91. The upper panels show the distribution of maximum water surface elevations. The lower panels show the time series of water surface elevations at tide stations. . . . .	22
10	Model results for mega-tsunami scenario SSSZ 1-10. The upper panels show the distribution of maximum water surface elevations. The lower panels show the time series of water surface elevations at tide stations. . . . .	22
11	Model results for Mw 7.5 scenario ATSZ B52. The upper panels show the distribution of maximum water surface elevations. The lower panels show the time series of water surface elevations at tide stations. . . . .	23
12	Maximum water surface elevations in micro-tsunami scenario SSSZ B11 simulated by the forecast model. . . . .	24
B1	Atlantic Source Zone unit sources. . . . .	29
B2	South Sandwich Islands Subduction Zone. . . . .	34
C1	Response of the Morehead City forecast model to synthetic scenario ATSZ 38-47 ( $\alpha=25$ ). Maximum sea surface elevation for (a) A grid, (b) B grid, and (c) C grid. Sea surface elevation time series at the C-grid warning point (d). The lower time series plot is the result obtained during model development and is shown for comparison with test results. . . . .	38

C2	Response of the Morehead City forecast model to synthetic scenario ATSZ 48-57 (alpha=25). Maximum sea surface elevation for (a) A grid, (b) B grid, and (c) C-grid. Sea surface elevation time series at the C-grid warning point (d). The lower time series plot is the result obtained during model development and is shown for comparison with test results. . . . .	39
C3	Response of the Morehead City forecast model to synthetic scenario SSSZ 1-10 (alpha=25). Maximum sea surface elevation for (a) A grid, (b) B grid, and (c) C grid. Sea surface elevation time series at the C-grid warning point (d). The lower time series plot is the result obtained during model development and is shown for comparison with test results. . . . .	40

## List of Tables

1	MOST setup of the reference and forecast models for Morehead City, North Carolina. . . . .	25
2	Synthetic tsunami scenarios employed to test the Morehead City, North Carolina reference and forecast models. . . . .	26
B1	Earthquake parameters for Atlantic Source Zone unit sources. . . . .	30
B2	Earthquake parameters for South Sandwich Islands Subduction Zone unit sources. . . . .	35
C1	Table of maximum and minimum amplitudes (cm) at the Morehead City warning point for synthetic and historical events tested using SIFT 3.2 and obtained during development. . . . .	41

**Abstract** This report documents the development, validation, and stability testing of a tsunami forecast model for Morehead City, North Carolina. The model is to be integrated into NOAA's short-term tsunami forecast system. In this system, tsunami propagation in nearshore waters and any subsequent runup on land are simulated in real time using the Method of Splitting Tsunami numerical model. The simulations are conducted using three grids at successively finer resolutions. The innermost grid covers Morehead City and the surrounding vicinity at a spatial resolution of approximately 62 meters. The model can complete a 12-hour simulation within 30 minutes of CPU time. Accuracy of the forecast model is evaluated by comparing the computational results to a high-resolution reference model in a series of scenarios. Numerical stability is also considered using these the synthetic mega- and micro-tsunami events.

## 1 Background and Objectives

The National Oceanic and Atmospheric Administration (NOAA) Center for Tsunami Research (NCTR) at the Pacific Marine Environmental Laboratory (PMEL) has developed a tsunami forecasting capability for operational use by NOAA’s two Tsunami Warning Centers located in Hawaii and Alaska (Titov et al., 2005). The system, termed Short-term Inundation Forecasting of Tsunamis (SIFT), is designed to efficiently provide basin-wide warning of approaching tsunami waves accurately and quickly. It combines real-time tsunami measurements with numerical models to produce estimates of tsunami wave arrival time and amplitudes at coastal communities of interest. This system integrates several key components: deep-ocean observations of tsunamis in real time, a basin-wide pre-computed propagation database of water level and flow velocities for potential seismic unit sources, an inversion algorithm to refine the tsunami source based on deep-ocean observations during an event, and inundation forecast models run in real time and at high resolutions for selected coastal communities.

Morehead City is a port city of the state of North Carolina. It has a land area of 17.74 km<sup>2</sup> and a population of 8664 (U.S. Census Bureau, 2010). The city was named after John Motley Morehead, the 29th governor of North Carolina. In the early 1850s, the town site was purchased by the Shepard Point Land Company with plans to use it as a transportation hub connecting the deep channel through Beaufort Inlet with the railroad. The city experienced a steady demographic and economic growth because of the deep-water port built at Shepard’s Point, as well as from the Atlantic and North Carolina Railroad that connected it to other parts of the state. The town was incorporated in 1861. Its growth was interrupted by the American Civil War, in which it was occupied by the federal troops (<http://moreheadcity.nc.gov/morehead-city-nc-history>). The city’s resurgence was brought by the construction of the Atlantic Hotel in the 1880s. Following the Great Depression and World War II, Morehead City experienced a downturn, deteriorating continuously until the 1980s, when the city received a community development block grant to replace an aging infrastructure and improve the waterfront area. This renewal has been maintained by governmental grants and private investments in the past decades. In 2003, the Morehead City Historic District was listed on the National Register of Historic Places.

Situated on the “Crystal Coast,” Morehead City is a popular destination for tourists. Tourism is a major component of the city’s economy, together with fishing and light industry. It is home to several marine research facilities, including the Institute of Marine Science and the Division of Marine Fisheries of the North Carolina Department of Transportation.

Morehead City may be subject to tsunamis caused by the earthquakes around the Atlantic Basin, especially those along the eastern edge of the Caribbean Plate and the eastern edge of the Scotia Plate. Besides earthquakes, submarine and subaerial landslides may also trigger tsunamis that could pose a threat to U.S. East Coast cities, including Morehead City (e.g., Driscoll et al., 2000; Ten Brink et al., 2008; Løvholt et al., 2008; Zhou et al., 2011).

In this study, we develop a tsunami forecast model for Morehead City. This model is to be integrated into NOAA’s tsunami forecast system as a part of its effort to provide a nationwide tsunami forecast capability.

## 2 Forecast Methodology

The main objective of a tsunami forecast model is to provide a quick and accurate estimate of tsunami arrival time, wave heights, and inundation during a tsunami event. Models are designed and tested to perform under stringent time constraints, given that time is generally the single limiting factor in saving lives and property. A forecast model relies on a high-resolution numerical model, which employs the Method of Splitting Tsunami (MOST) to simulate the nearshore propagation and runup in real time. MOST solves the shallow water equations through a finite difference scheme. The numerical code has been validated extensively against laboratory experiments (Synolakis et al., 2008).

Simulating tsunami propagation in an ocean basin is, computationally, very time-consuming. Instead of real-time simulation, the oceanic propagation is estimated through the linear combination of tsunami source functions. A tsunami source function is the time series of water surface elevations and velocities in an oceanic basin due to a unit earthquake source, which measures  $100 \times 50 \text{ km}^2$  in area and has a slip value of 1 m, equivalent to the moment magnitude ( $M_w$ ) of 7.5 (Gica et al., 2008). Unit earthquake sources have been constructed to encompass all areas where potentially tsunamigenic subduction zones exist. The tsunami source function for each unit earthquake source is pre-computed with MOST at a 4-arc-min resolution and stored in a tsunami propagation database. Given that tsunami evolution in the deep ocean is a linear process (Kânoğlu and Synolakis, 2006), a tsunami scenario can be accurately represented through the linear combination of related source functions. During a tsunami event, as the tsunami waves propagate across the ocean and successively reach the DART (Deep-Ocean Assessment and Reporting of Tsunamis) observation sites, recorded sea level is ingested into the tsunami forecast application in near real time and incorporated into an inversion algorithm to produce an improved estimate of the tsunami source (Percival et al., 2011).

Since nonlinear effects are stronger in nearshore tsunami evolution, these processes are simulated with MOST in real time. A tsunami forecast model consists of three telescoped grids with successively finer resolutions. The seaward boundaries of the outermost A grid are placed in deep water. Pre-computed boundary conditions are input along these boundaries to force the real-time simulations. The B grid is an intermediate grid that provides a transition between the outermost A grid and the innermost C grid. The C grid covers the population and economic center of the at-risk community. Due to shoaling effects, waves become short when they approach shorelines. High resolution is needed for the C grid to sufficiently represent the bathymetric and topographic features, as well as to accurately resolve and simulate nearshore tsunami evolutions. Bathymetric and topographic grids are derived from digital elevation models (DEMs) developed by the National Geophysical Data Center (NGDC) and NCTR. Technical aspects of forecast model development, validation, and stability testing have been reported by Titov and González (1997), while Tang et al. (2009) provides details of the forecast methodology.

Forecast models, including that of Morehead City, are constructed for at-risk coastal communities in the Pacific and Atlantic oceans. Previous studies have validated the accuracy and efficiency of each forecast model currently implemented in the real-time tsunami forecast system (Titov et al., 2005; Titov, 2009; Tang et al., 2008; Wei et al., 2008).

### 3 Model Development

Accurate forecast of tsunami impact on a coastal community largely relies on the accuracy of the bathymetric and topographic data. The basis for the development of the grids in a tsunami forecast model is the high-resolution DEMs. For each community, the DEMs are compiled from a variety of recent data sources. All these data have been shifted to the World Geodetic System 1984 horizontal datum, and the vertical datum of Mean High Water. A high-resolution “reference” model is first developed. From this, an “optimized” model is constructed by downgrading the resolution and reducing the domain coverage of the reference model grids. The purpose of this optimization is to reduce the required CPU time to an operationally specified period, which is no more than 10 min for a 4-hr simulation. This operationally developed model is referred to as the optimized tsunami forecast model, or simply the “forecast model.” In the development of a forecast model, the computational results are carefully compared to the reference model to check if due accuracy is maintained.

#### 3.1 Forecast area

Figure 1 shows a map of Morehead City and the surrounding vicinity. The semi-closed Bogue Sound separates Bogue Banks from mainland Carteret County, where Morehead City is located. The sound is a portion of the Atlantic Intercontinental Waterway. Vessels enter the sound through both Beaufort Inlet in the east and Bogue Inlet (not shown in the figure) in the west. Offshore of Bogue Banks is the continental shelf, over which the water depth increases slowly to approximately 50 m over nearly 100 km. When a long wave such as a tsunami propagates over the continental shelf, a great amount of wave energy can dissipate due to bottom friction. The continental shelf and low-lying coastal islands form a natural barrier for Morehead City. As a result, the city has experienced very few hazardous waves in history. As wave speeds decrease with water depth, the wide continental shelf also delays the arrival of tsunamis in the present forecast area. This requires that the real-time simulation in the forecast model be conducted for a longer period.

#### 3.2 Digital elevation models

The bathymetry and topography used in the development of this forecast model was based on a DEM provided by NGDC that the author considers to be an adequate representation of the local topography and bathymetry. As new DEMs become available, forecast models will be updated and report updates will be posted at [http://nctr.pmel.noaa.gov/forecast\\_reports](http://nctr.pmel.noaa.gov/forecast_reports).

The Atlantic Basin is covered by a 1-min bathymetric grid from 72°S to 72°N in latitude and from 20°E to 105°W in longitude. The grid was compiled by merging the 1 min grid from the General Bathymetric Chart of the Ocean ([https://www.bodc.ac.uk/data/online\\_delivery/gebco/gebco\\_one\\_minute\\_grid/](https://www.bodc.ac.uk/data/online_delivery/gebco/gebco_one_minute_grid/)) with measured and estimated seafloor topography grids in areas of water depth greater than 200 m.

For the U.S. East Coast, NGDC has developed a 9-arc-sec grid that spans from 25°N to 50°N in latitude and from 85°W to 50°W in longitude. These data were compiled from a variety of data sources including the multibeam bathymetry surveys performed by the

National Ocean Service (NOS), NOAA Ocean Exploration, the U.S. Geological Survey, and other agencies; hydrographic survey data from NOS; and Lidar data collected by the Joint Airborne Lidar Bathymetry Technical Center of Expertise.

For Morehead City and the surrounding vicinity, there is a 1/3-arc-sec DEM that covers areas from 34.37°N to 35.57°N in latitude and from 77.27°W to 76.0°W in longitude (Grothe et al., 2011). A zero contour line was first created to represent the latest coastline based on Google Earth satellite imagery from 2011. Bathymetric data were sourced from the NOS hydrographic survey, the U.S. Army Corps of Engineers hydrographic channel surveys, and the multibeam swath sonar survey conducted by the North Carolina Department of Environment and Natural Resources. The bathymetry-topography datasets employed by NGDC include the DEM developed by the North Carolina Department of Environment and Natural Resources, and the data published by the Coastal Service Center of the U.S. Army Corps of Engineers in 2004. The topographic data are derived from the U.S. Geological Survey 1/3-arc-sec National Elevation Dataset DEM, and the North Carolina Department of Emergency Management Floodplain Mapping Program Lidar.

### 3.3 Grid setup

In Figure 2, we present the extents of grids in the forecast model. The offshore boundaries of the A grid extend into the deep ocean. Pre-computed boundary conditions for this grid are derived by linearly combining tsunami source functions from the pre-computed propagation database. The west and north boundaries intersect the continental shelf. Given that waves may become very nonlinear in shallow water, the input boundary conditions may become inaccurate in these regions. This problem can be magnified if the alongshore wave propagation is strong. A solution to this problem is to put these boundaries far from the area of interest. The B grid provides a transition of real-time simulations between the A and C grids. In the forecast model, the B grid covers a region over most areas of the continental shelf offshore of Morehead City. The C grid covers the entire Morehead City area and its vicinity. As noted in Section 2, waves in this grid may undergo complicated processes of diffraction, reflection, and shoaling due to shallow water depth and complex coastlines. Very high resolution is applied on this level to better capture the physical features. In the present forecast area, there is a tide gauge that has been operated by NOS in Beaufort Harbor (34°43.2'N, 76°40.2'W) since 10 June 1990, and a tide gauge installed near Spooners Creek (34°43.5'N, 76°48.2'W) on 25 March 2012. The water depth is 2.49 m and 0.70 m for the Beaufort Harbor and Spooners Creek tide stations, respectively. These stations are also denoted in Figure 2.

The limits of the reference and forecast model grids are plotted in Figures 3 and 4. Parameters of both models are presented in Table 1. In both models, simulations are initiated when the input water surface displacement reaches a threshold of 0.001 m along the open boundaries of A grids. To approximate the energy dissipation due to seabed friction, we employ a constant Manning's roughness coefficient of 0.03, a typical value for coastal waters (Bryant, 2001), in all grids. We note that by employing this coefficient on the dry land covered by vegetation, we may underestimate the friction forces and, as a result, over-predict the runup.

## 4 Model Testing

Before it is integrated into NOAA’s tsunami forecast system, the accuracy and stability of a forecast model is stringently tested. Accuracy of a numerical model may be compromised by inaccurate bathymetry and topography, as well as numerical dispersion. The latter is inherent of finite difference schemes, as employed by MOST, and depends on the spatial resolution of grids.

While an accurate model largely dictates the reliability of a tsunami forecast, unforeseen instabilities may still cause a forecast to fail. Given the intention to employ the model for an operational application, the robustness of the model should be carefully evaluated so that instabilities are avoided beforehand as much as possible. Due to the lack of historical tsunami records in the Morehead City area, the forecast model cannot be validated for real events. Therefore, in this section, we assess the accuracy of the forecast model by using several synthetic scenarios. These scenarios also allow the stability of the model to be checked.

### 4.1 Accuracy

The U.S. East Coast, where Morehead City is situated, is thought to be at risk from tsunamis generated by earthquakes that may occur in the subduction zones along the eastern edge of the Caribbean Plate and the eastern edge of the Scotia Plate. In this section, we synthesize several scenarios that represent possible earthquakes in these zones. The scenarios include six “mega” (Mw 9.3) tsunamis, along with a tsunami generated by a Mw 7.5 earthquake. The parameters of these scenarios are presented in Table 2. Epicenters of earthquakes that trigger the mega-tsunamis are plotted in Figure 4.

In Figures 5–11, we present the modeling results of the synthetic scenarios. All the simulations are conducted for 12 hr. In general, the reference and forecast models show close agreement at the Beaufort station location. As the Spooners Creek station is closer to the shoreline, the more complex dynamics of simulations at this location show greater sensitivity to grid resolutions, and therefore display bigger differences between the two models. Agreement is better for the leading waves when the wavelength is long. But since numerical errors increase for shorter waves, bigger differences are observed in trailing waves when their wavelengths are relatively short. The maximum runup is usually attributed to the longer waves, therefore numerical errors in shorter waves may not significantly affect the forecast of coastal runup.

Maximum water surface elevations over the area covered by the forecast model’s C grid are also compared between the forecast and reference models in Figures 5–11. Maps of maximum water surface elevations serve as indicators of which locations might experience the most severe tsunami impact. In all scenarios, close agreement is observed for the maps of maximum water surface elevations for both models, suggesting that the forecast model is reasonably accurate.

Due to the loss of energy as waves encounter higher seabed friction over the continental shelf, the wave heights are significantly lowered in the Morehead City forecast area. The most severe mega-tsunami scenario is ATSZ 48-57 (Figure 6), where the maximum wave height is approximately 0.4 m at the Spooners Creek tide gauge station and 0.8 m at the Beaufort Harbor tide gauge station. In this event, Bogue Banks is mostly flooded. Bogue Banks and

small offshore islands effectively reduce the wave heights in Bogue Sound, protecting the coast of Morehead City. In this scenario, waves may break nearshore and on the dry land. MOST neglects the energy dissipation due to wave breaking. As a result, runup may be significantly overestimated.

In some mega-tsunami event scenarios, for example ATSZ 68-77 (Figure 8), the highest waves are present in the wave groups that arrive in the Morehead City area several hours after the first waves. These trailing waves may cause the most severe flooding in this area, so it is of critical importance to ensure the stability of the simulation for up to 12 hr after initiated.

## 4.2 Stability

Very large incoming waves may generate instability within a numerical model. A widely practiced solution to this issue is to reduce the time step. The synthetic mega-tsunami events represent the most severe tsunamis that may hit the forecast area. Figures 5–11 show that there is no instability observed in these scenarios.

Instability may also be caused even when incoming waves are very small. In this situation, the amplitude of numerical noise or instabilities may be as great as or even larger than the actual sea-level variability. Numerical noise can accumulate, amplify, and ultimately cause the failure of the computation. In this report, we test the forecast model against a synthetic micro-tsunami (Mw 6.1) scenario (see SSSZ B11 in Table 2). The incoming waves are smaller than the threshold to initiate forecast computation (see Appendix A). Under operational conditions, a forecast model would not be initiated for such an event. Therefore, we temporarily lower this threshold to 0.00001 m. The forecast model performs a 12-hr simulation without evidence of any instability. In Figure 12, we plot the maximum water surface elevations in the three grids in the forecast model. All the tests conducted in this report indicate that numerical instability is unlikely to cause the failure of the forecast model in a real event.

## 5 Conclusions

In this study, we have developed a tsunami forecast model for Morehead City, North Carolina. The model is to be integrated into NOAA’s short-term tsunami inundation forecast system. The forecast model is based on the MOST numerical model, which simulates tsunami propagation and runup in the forecast area through three telescoped grids in real time. Morehead City and the surrounding vicinity are covered by the innermost grid at a spatial resolution of approximately 62 m. The forecast model is designed and configured such that it will complete a 12-hr simulation within 30 min of CPU time.

Since there are no historical records of tsunamis at Morehead City, the accuracy of the forecast model is evaluated using several synthetic tsunami scenarios. Good agreement between the forecast and reference models for each of these scenarios indicates any numerical errors resulting from the forecast model’s relatively coarse resolutions are unlikely to significantly diminish the accuracy of the forecast results. The forecast model was also tested for synthetic mega- and micro-tsunami scenarios. No stability issue was observed in any of these simulations.

## **Acknowledgments**

This work is funded by the Joint Institute for the Study of the Atmosphere and Ocean (JISAO) under NOAA Cooperative Agreement Numbers NA10OAR4320148 and NA08OAR4320899 and is JISAO contribution number No. 2099. This work is also Contribution No. 3413 from NOAA/Pacific Marine Environmental Laboratory (PMEL). The author thanks S. Bigley of PMEL for helpful revision recommendations.

## References

- Bryant, E. (2001), *Tsunami: the Underrated Hazard*, Cambridge University Press, 320 pp.
- Driscoll, N. W., Weissel, J. K., and Goff, J. A. (2000), Potential for large-scale submarine slope failure and tsunami generation along the U.S. mid-Atlantic coast, *Geology*, *20*(5), 4407–4410.
- Gica, E., Spillane, M. C., Titov, V. V., Chamberlin, C. D., and Newman, J. C. (2008), Development of the forecast propagation database for NOAA's Short-Term Inundation Forecast for Tsunamis (SIFT), *NOAA Tech. Memo. OAR PMEL-139*, Pacific Marine Environmental Laboratory, NOAA, Seattle, WA, 89 pp.
- Grothe, P. G., Taylor, L. A., Eakins, B. W., Carignan, K. S., Friday, D. Z., Lim, E., and Love, M. (2011), Digital elevation models of Morehead City, North Carolina: Procedures, data sources and analysis, National Geophysical Data Center, NOAA, Boulder, CO, 22 pp.
- Kânoğlu, U., and Synolakis, C.E. (2006). Initial value problem solution of nonlinear shallow water wave equations, *Phys. Rev. Lett.*, *97*(14), 148501, doi:10.1103/PhysRevLett.97.148501.
- Løvholt, F., Pedersen, G., and Gisler, G. (2008), Oceanic propagation of a potential tsunami from the La Palma Island, *J. Geophys. Res.*, *113*, C09026, doi:10.1029/2007JC004603.
- Percival, D. B., Denbo, D. W., Eble, M. C., Gica, E., Mofjeld, H. O., Spillane, M. C., Tang, L., and Titov, V. V. (2011). Extraction of tsunami source coefficients via inversion of DART<sup>®</sup> buoy data, *Nat. Hazards*, *58*(1), doi: 10.1007/s11069-010-9688-1, 567–590.
- Synolakis, C. E., Bernard, E. N., Titov, V. V., Kânoğlu, U., and González, F. I. (2008): Validation and verification of tsunami numerical models, *Pure Appli. Geophys.*, *165*(11-12), 2197–2228.
- Tang, L., Titov, V. V., Wei, Y., Mofjeld, H. O., Spillane, M., Arcas, D., Bernard, E. N., Chamberlin, C. D., Gica, E., and Newman, J. (2008), Tsunami forecast analysis for the May 2006 Tonga tsunami, *J. Geophys. Res.*, *113*, C12015, doi: 10.1029/2008JC004922.
- Tang L., Titov, V. V., and Chamberlin, C. D. (2009), Development, testing, and applications of site-specific tsunami inundation models for real-time forecasting, *J. Geophys. Res.*, *6*, doi: 10.1029/2009JC005476.
- Ten Brink, U., Twichell, D., Geist, E., Chaytor, J., Locat, J., Lee, H., Buczkowski, B., Barkan, R., Solow, A., Andrews, B., Parsons, T., Lynett, P., Lin, J., and Sansoucy, M. (2008), Evaluation of tsunami sources with the potential to impact the U.S. Atlantic and Gulf coasts, USGS Administrative Report to the Nuclear Regulatory Commission, 300 pp.
- Titov, V. V. and González, F. I. (1997), Implementation and testing of the Method of Splitting Tsunami (MOST) model, *NOAA Tech. Memo, ERL PMEL-112*, Pacific Marine Environmental Laboratory, NOAA, Seattle, WA, 11 pp.

- Titov V. V., González F. I., Bernard E. N., Eble M. C., Mofjeld H. O., Newman J. C., and Venturato A. J. (2005), Real-time tsunami forecasting: challenges and solutions, *Nat. Hazards*, 35, 41–58.
- Titov, V. V. (2009), Tsunami forecasting. In: E. N. Bernard and A. R. Robinson (edited) *The Sea*, Vol. 15, Chapter 12, Harvard University Press, Cambridge, MA, and London, U.K., 371–400.
- U.S. Census Bureau (2010), American FactFinder Fact Sheet: Morehead City, North Carolina, retrieved on 9 April 2014, from <http://quickfacts.census.gov/qfd/states/37/3744320.html>.
- Wei, Y., Bernard, E. N., Tang, L., Weiss, R., Titov, V. V., Moore, C., Spillane, M., Hopkins, M., and Kânoğlu, U. (2008), Real-time experimental forecast of the Peruvian tsunami of August 2007 for U.S. coastlines, *Geophys. Res. Lett.*, 35, L04609, doi:10.1029/2007GL032250.
- Zhou, H., Moore, C. W., Wei, Y., and Titov, V. V. (2011), A nested-grid Boussinesq-type approach to modelling dispersive propagation and runup of landslide-generated tsunamis, *Nat. Hazards Earth Syst. Sci.*, 11(10), doi: 10.5194/nhess-11-2677-2011, 2677–2697.

## Figures

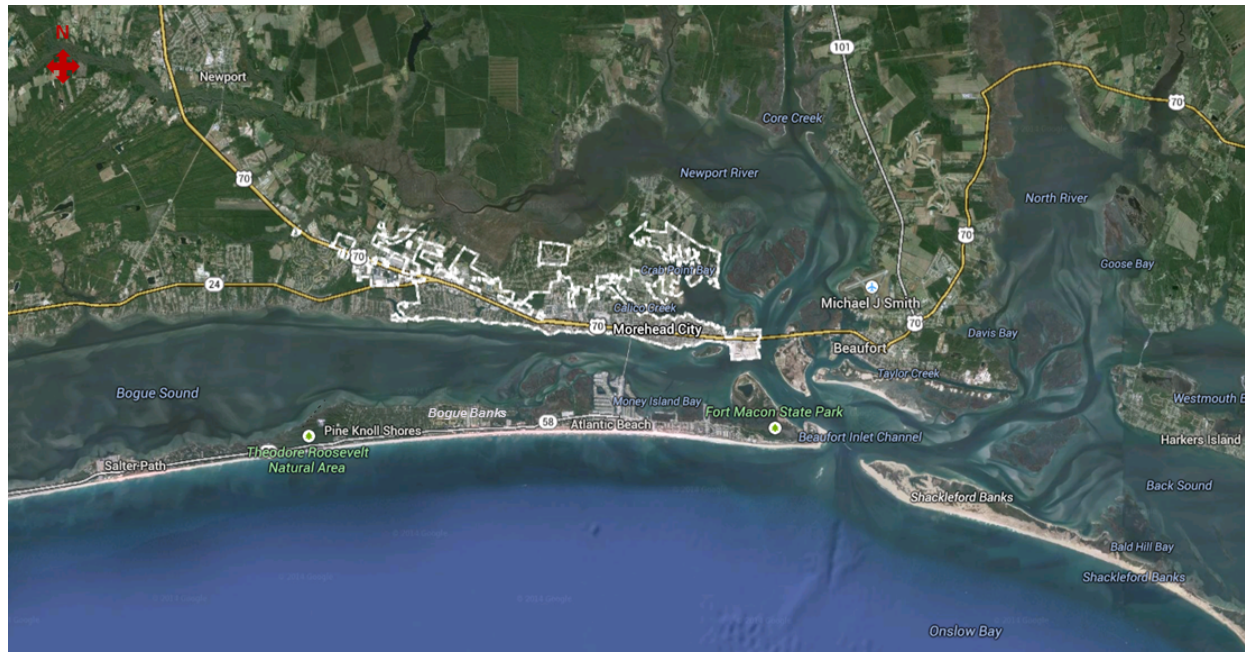


Figure 1: Morehead City, North Carolina, and the surrounding vicinity (courtesy of Google Maps).

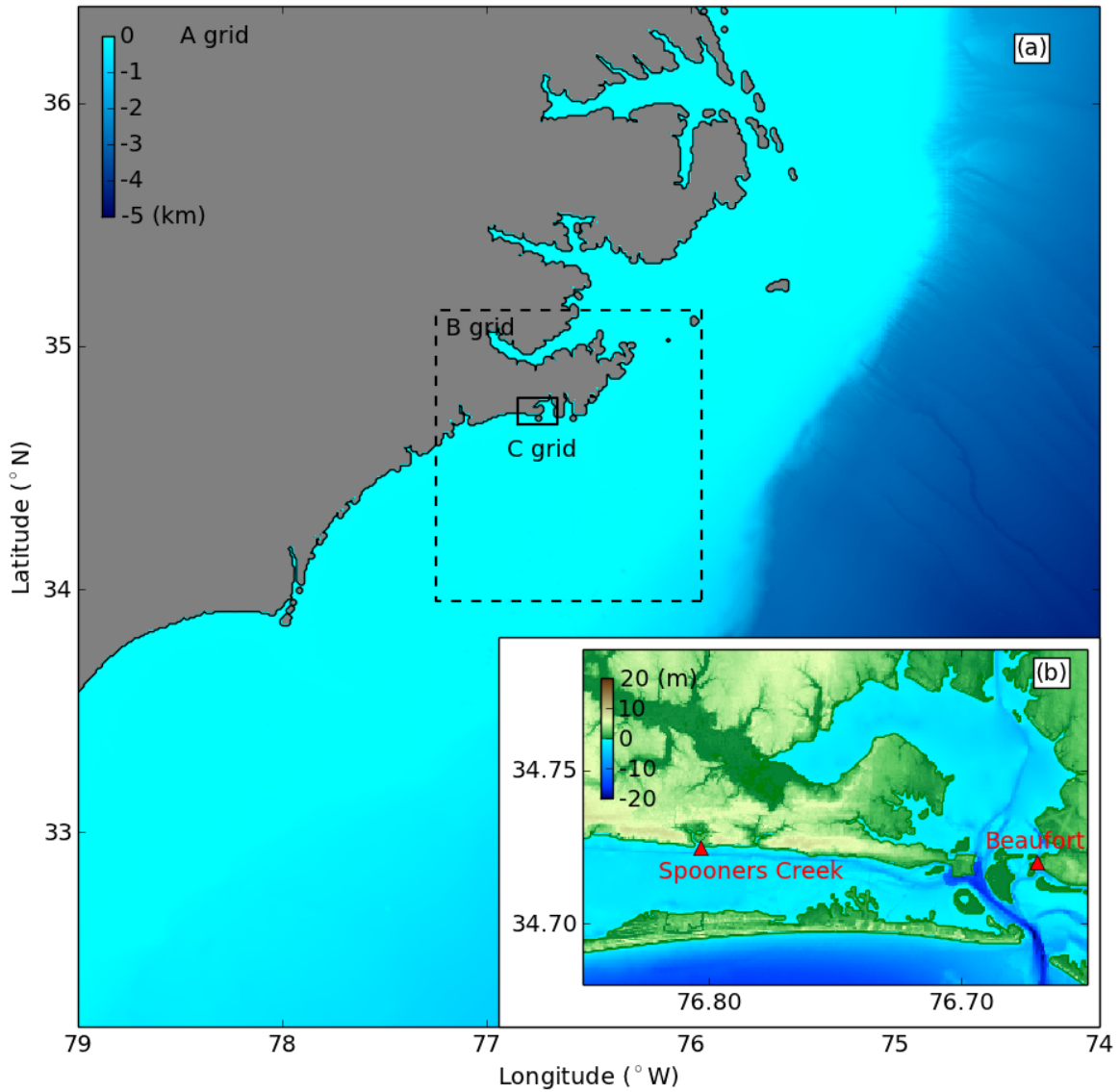


Figure 2: Grid extents of the Morehead City forecast model: (a) grid extents, (b) bathymetry and topography of the C grid. The triangles in the C grid denote the tide stations near Spooners Creek and Beaufort Harbor.

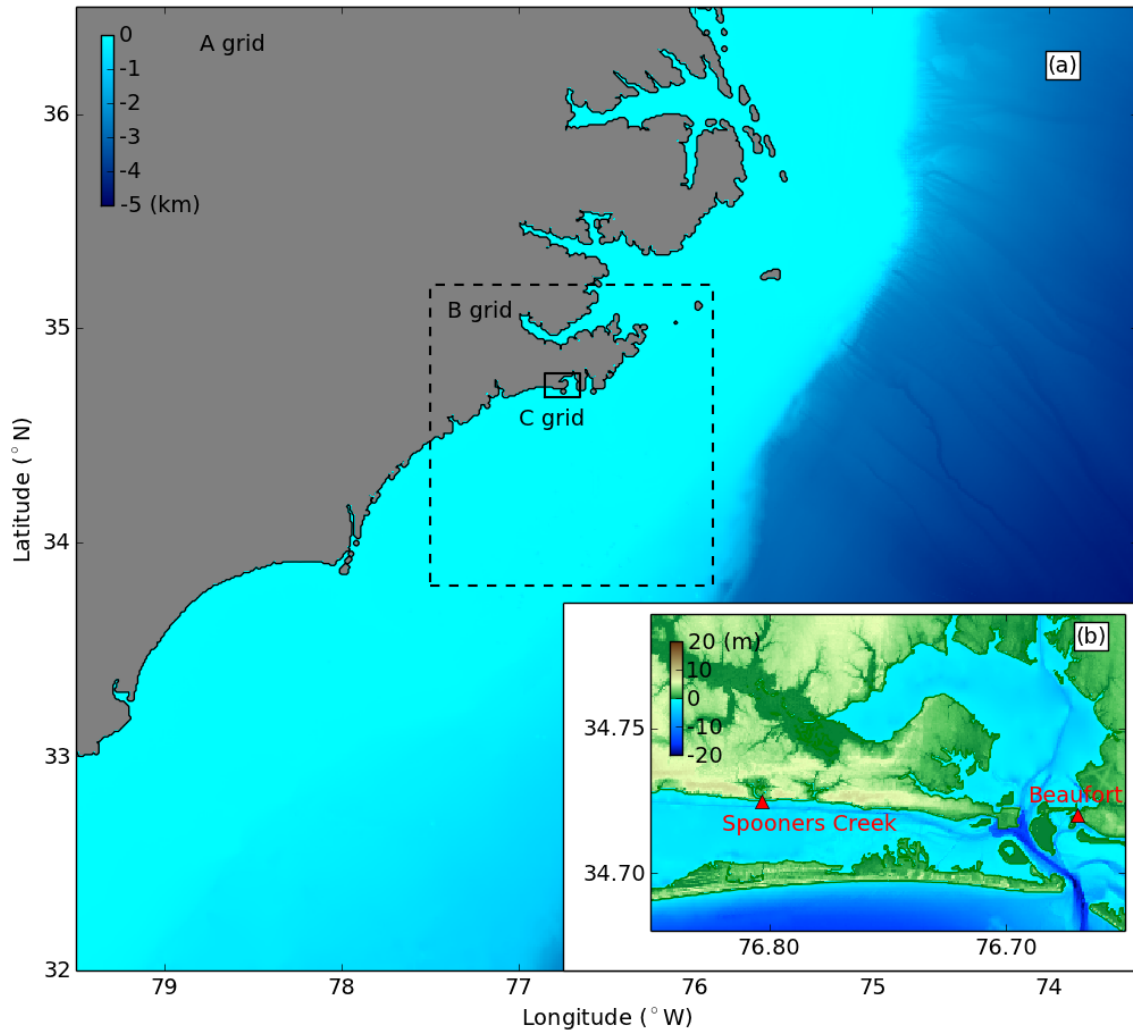


Figure 3: Grid extents of the Morehead City reference model: (a) grid extents, (b) bathymetry and topography of the C grid. The triangles in (b) denote the tide stations at Spooners Creek and Beaufort Harbor.

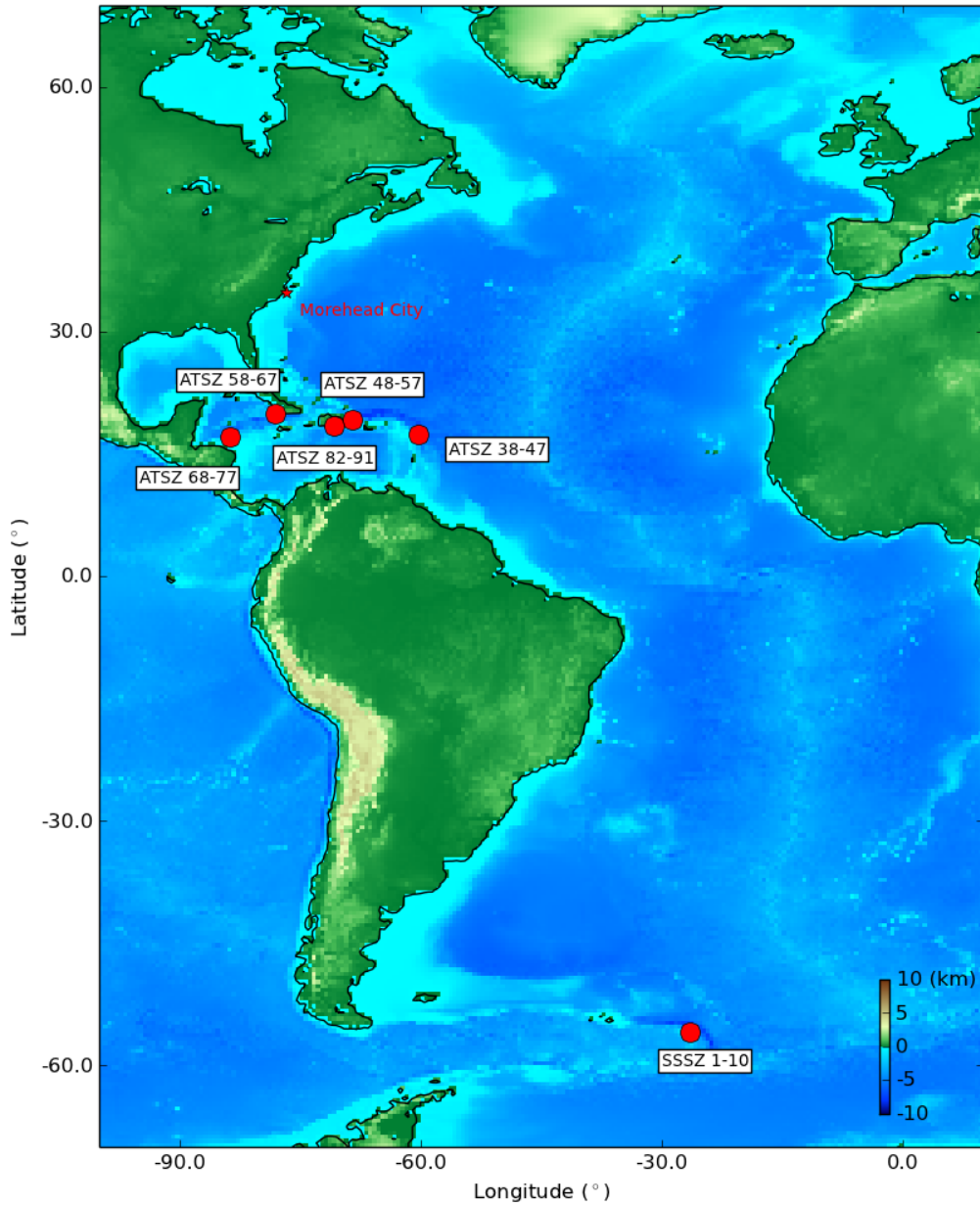


Figure 4: Epicenters of triggering earthquakes in synthetic mega-tsunami scenarios employed to test the Morehead City, North Carolina forecast and reference models. Location of Morehead City is indicated as a star in the map.

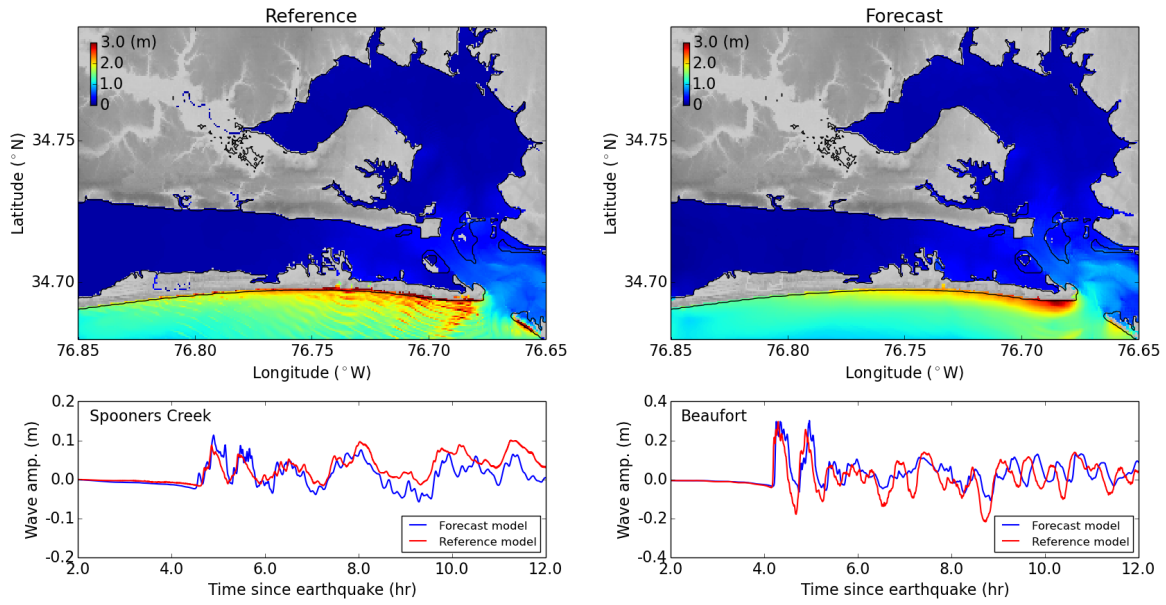


Figure 5: Model results for mega-tsunami scenario ATSZ 38-47. The upper panels show the distribution of maximum water surface elevations. The lower panels show the time series of water surface elevations at tide stations.

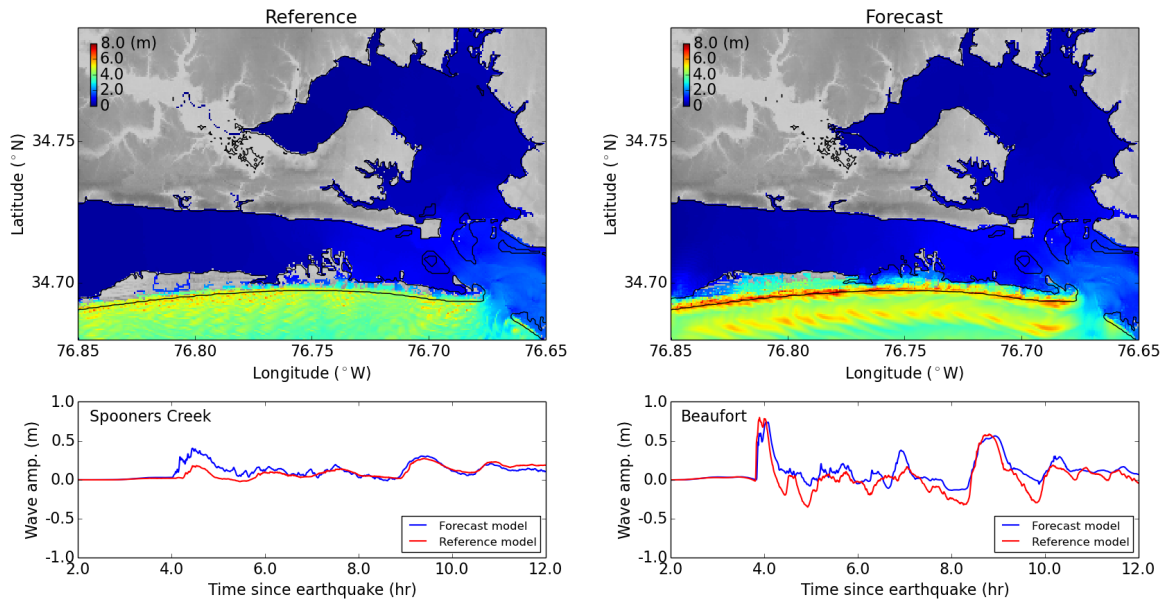


Figure 6: Model results for mega-tsunami scenario ATSZ 48-57. The upper panels show the distribution of maximum water surface elevations. The lower panels show the time series of water surface elevations at tide stations.

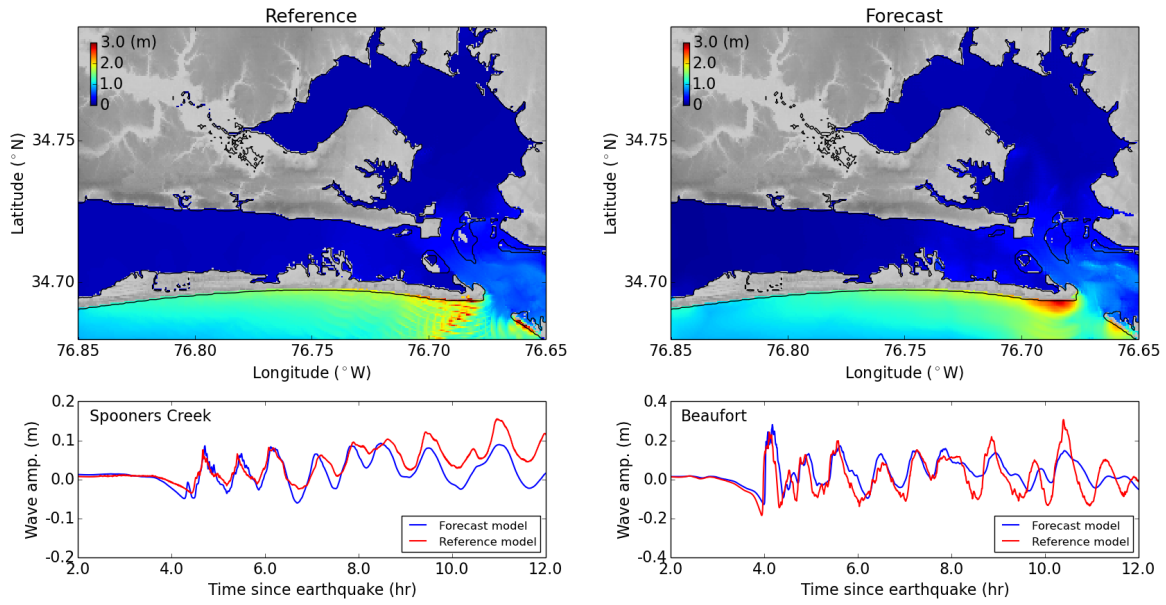


Figure 7: Model results for mega-tsunami scenario ATSZ 58-67. The upper panels show the distribution of maximum water surface elevations. The lower panels show the time series of water surface elevations at tide stations.

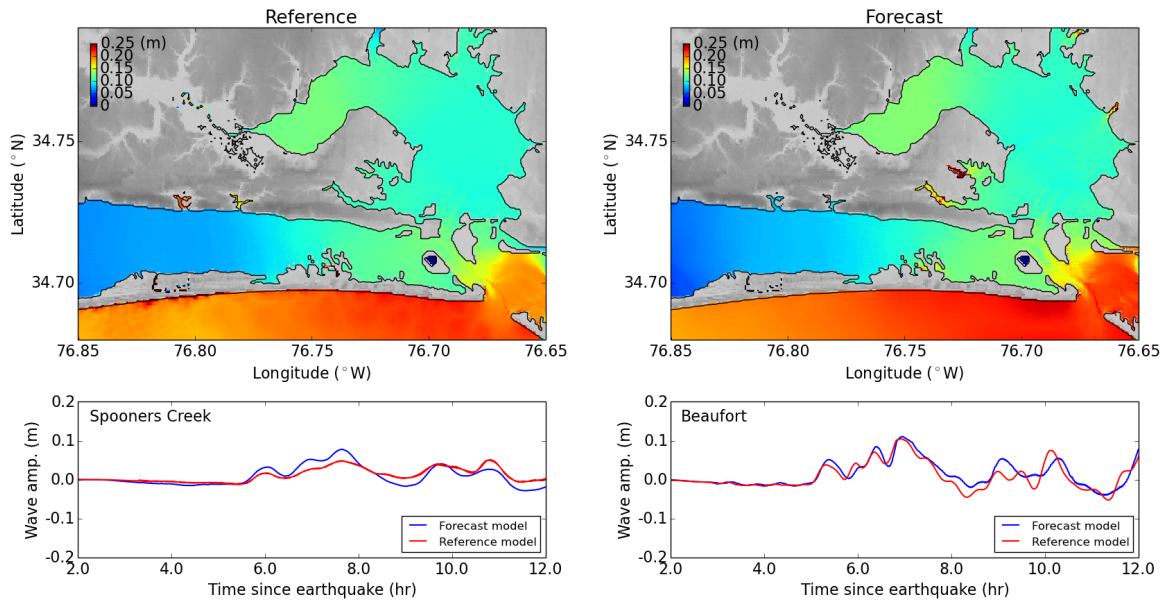


Figure 8: Model results for mega-tsunami scenario ATSZ 68-77. The upper panels show the distribution of maximum water surface elevations. The lower panels show the time series of water surface elevations at tide stations.

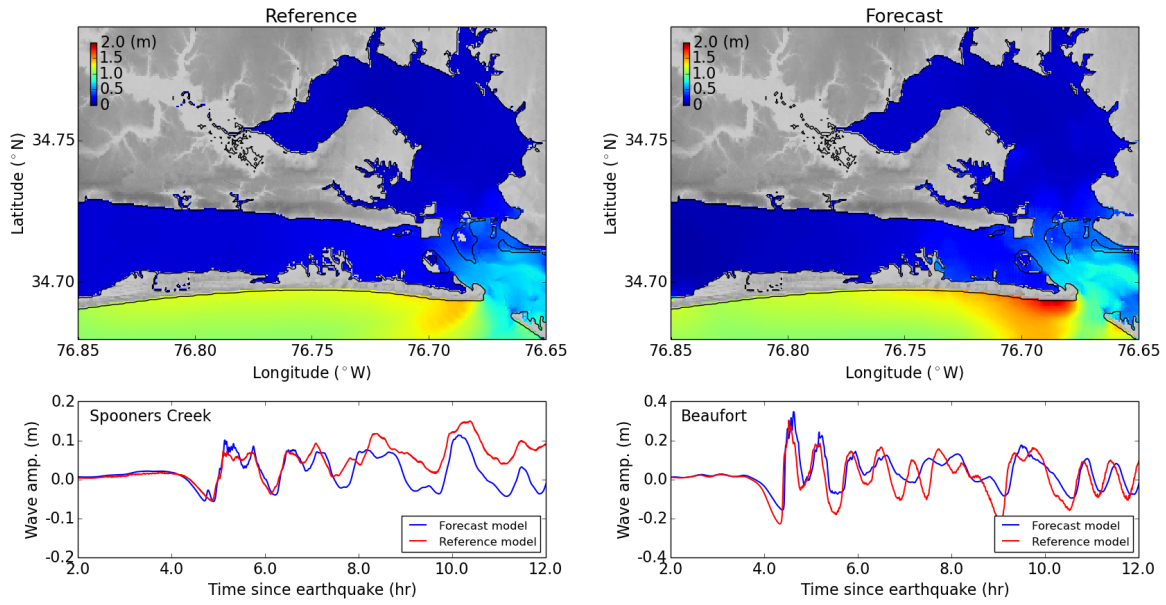


Figure 9: Model results for mega-tsunami scenario ATSZ 82-91. The upper panels show the distribution of maximum water surface elevations. The lower panels show the time series of water surface elevations at tide stations.

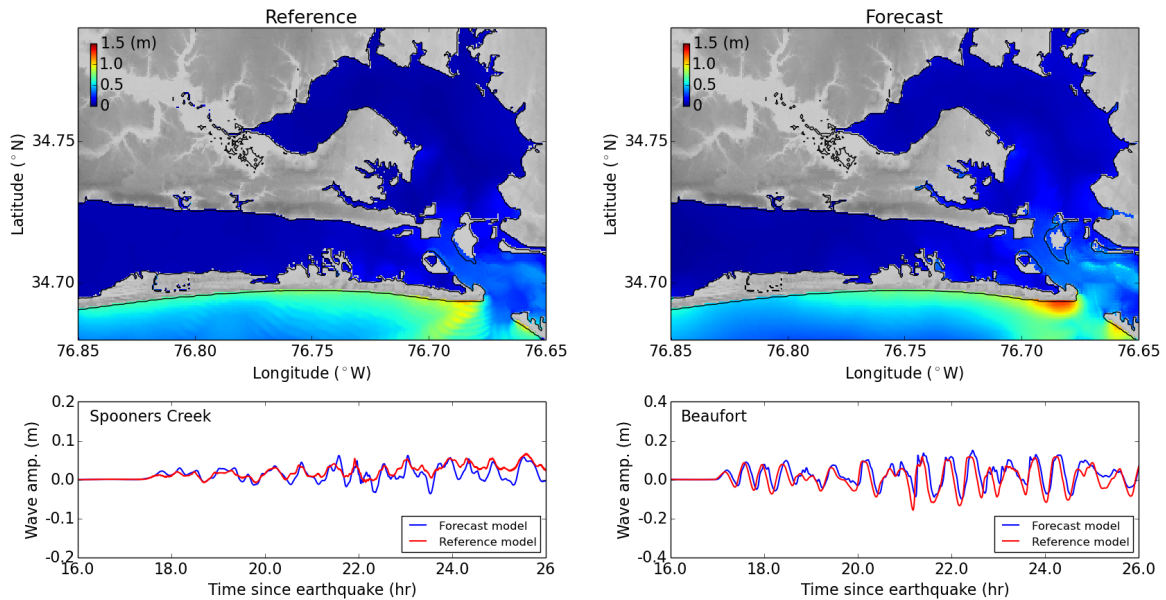


Figure 10: Model results for mega-tsunami scenario SSSZ 1-10. The upper panels show the distribution of maximum water surface elevations. The lower panels show the time series of water surface elevations at tide stations.

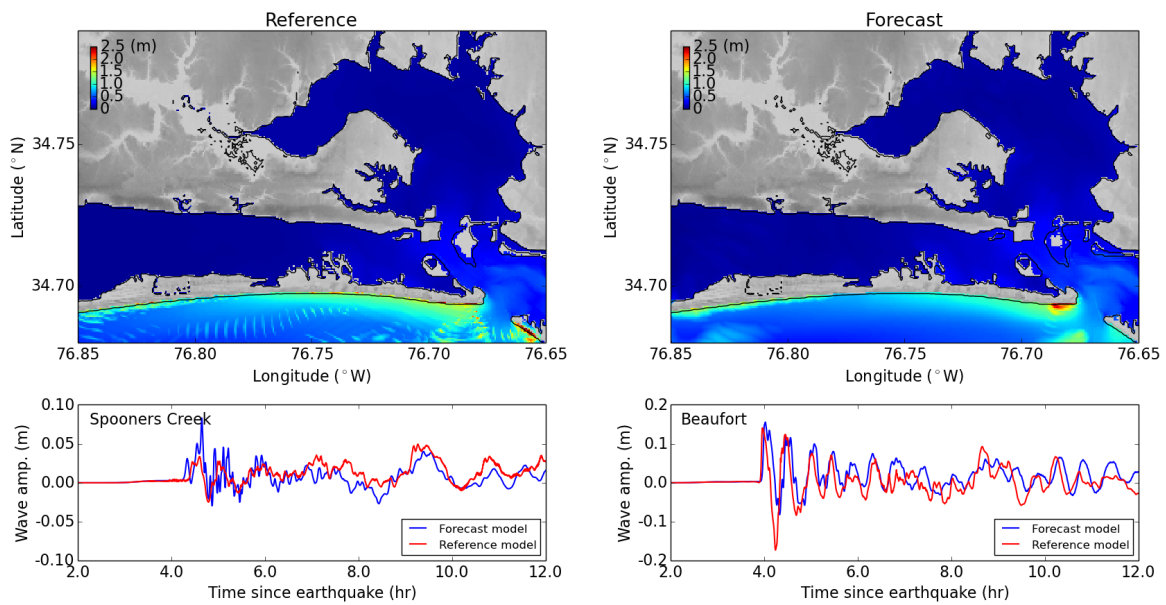


Figure 11: Model results for Mw 7.5 scenario ATSZ B52. The upper panels show the distribution of maximum water surface elevations. The lower panels show the time series of water surface elevations at tide stations.

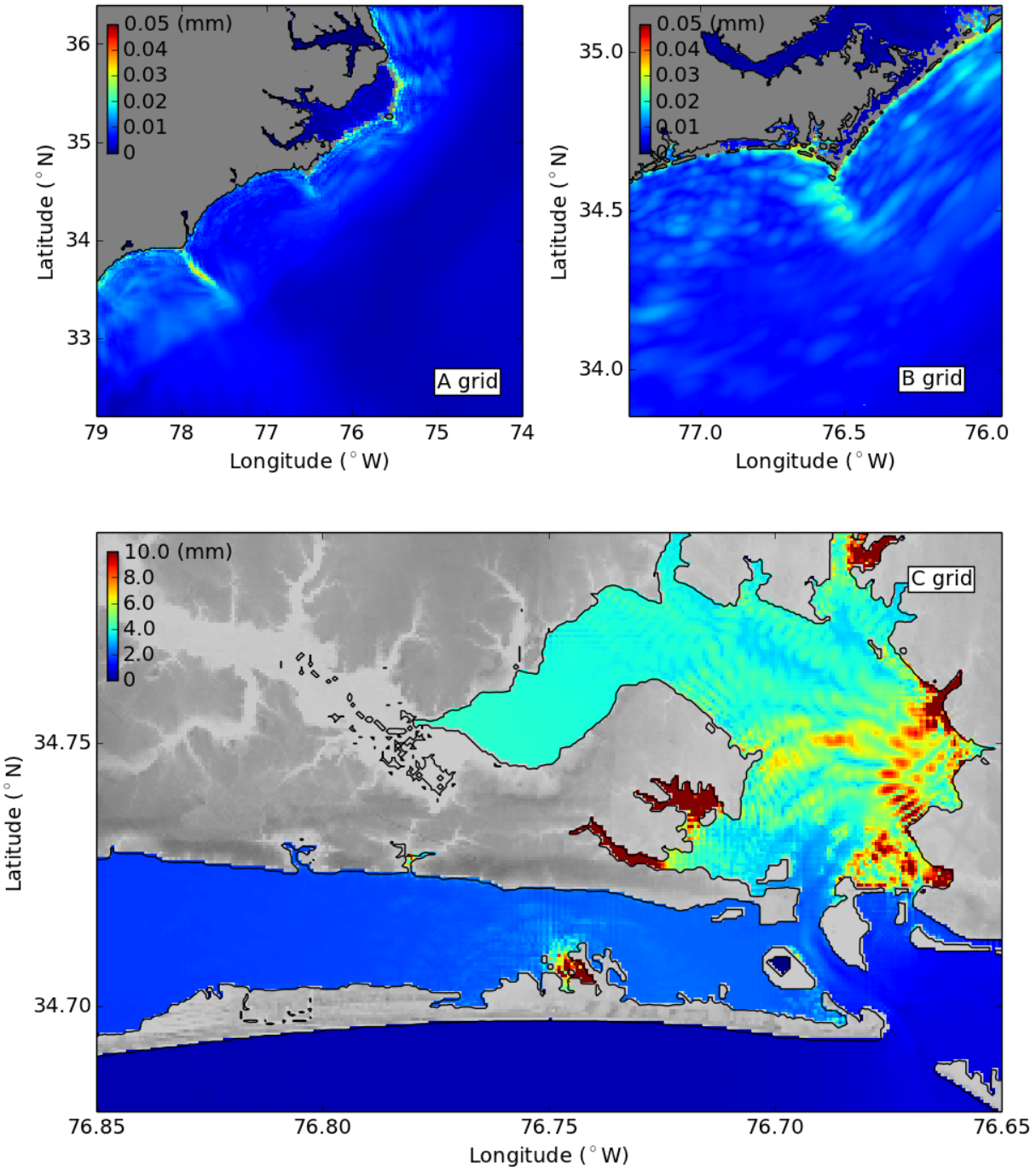


Figure 12: Maximum water surface elevations in micro-tsunami scenario SSSZ B11 simulated by the forecast model.

Table 1: MOST setup of the reference and forecast models for Morehead City, North Carolina.

Grid	Region	Reference Model				Forecast Model			
		Coverage Lat. ( $^{\circ}$ N) Lon. ( $^{\circ}$ W)	Cell Size Lat. Lon.	nx $\times$ ny	Time Step (sec.)	Coverage Lat. ( $^{\circ}$ N) Lon. ( $^{\circ}$ W)	Cell Size Lat. Lon.	nx $\times$ ny	Time Step (sec.)
A	Mid & South	32.0–36.5	30''	601 $\times$ 541	3.0	32.2–36.4	60''	251 $\times$ 253	7.5
	U.S. East Coast	79.5–73.5	36''			79.0–74.0	72''		
B	North Carolina	33.8–35.2	3.0''	1601 $\times$ 1681	0.6	33.85–35.15	10.0''	391 $\times$ 469	3.0
		77.5–75.9	3.6''			77.25–75.95	12.0''		
C	Morehead City	34.68–34.79	0.5''	1201 $\times$ 793	0.6	34.68–34.79	2.0''	301 $\times$ 199	1.5
		76.85–76.65	0.6''			76.85–76.65	2.4''		
Minimum offshore depth (m)					1.0	1.0			
Water depth for dry land (m)					0.1	0.1			
Friction coefficient ( $n^2$ )					0.0009	0.0009			
CPU time for a 12-hr simulation						< 30 min			

Table 2: Synthetic tsunami scenarios employed to test the Morehead City, North Carolina reference and forecast models.

Scenario No.	Scenario Name	Source Zone	Tsunami Source	$\alpha$ [m]
<b>Mega-tsunami Scenario</b>				
1	ATSZ 38-47	Atlantic	A38-A47, B38-B47	25
2	ATSZ 48-57	Atlantic	A48-A57, B48-B57	25
3	ATSZ 58-67	Atlantic	A58-A67, B58-B67	25
4	ATSZ 68-77	Atlantic	A68-A77, B68-B77	25
5	ATSZ 82-91	Atlantic	A82-A91, B82-B91	25
6	SSSZ 1-10	South Sandwich	A1-A10, B1-B10	25
<b>Mw 7.5 Scenario</b>				
7	ATSZ B52	Atlantic	B52	1
<b>Micro-tsunami Scenario</b>				
8	SSSZ B11	South Sandwich	B11	0.01

## A Model \*.in files for Morehead City, North Carolina

### A.1 Reference model \*.in file

0.001	Minimum amp. of input offshore wave (m)
1.0	Minimum depth of offshore (m)
0.1	Dry land depth of inundation (m)
0.0009	Friction coefficient ( $n^{**2}$ )
1	run up in a and b
300.0	max wave height meters
0.6	time step (sec)
72000	number of steps for 12 h simulation
5	Compute "A" arrays every n-th time step, n=
1	Compute "B" arrays every n-th time step, n=
50	Input number of steps between snapshots
0	...starting from
1	...saving grid every n-th node, n=

### A.2 Forecast model \*.in file

0.001	Minimum amp. of input offshore wave (m)
1.0	Minimum depth of offshore (m)
0.1	Dry land depth of inundation (m)
0.0009	Friction coefficient ( $n^{**2}$ )
1	run up in a and b
300.0	max wave height meters
1.5	time step (sec)
28800	number of steps for 12 h simulation
5	Compute "A" arrays every n-th time step, n=
2	Compute "B" arrays every n-th time step, n=
20	Input number of steps between snapshots
0	...starting from
1	...saving grid every n-th node, n=

**B Propagation Database:  
Atlantic Ocean Unit Sources**

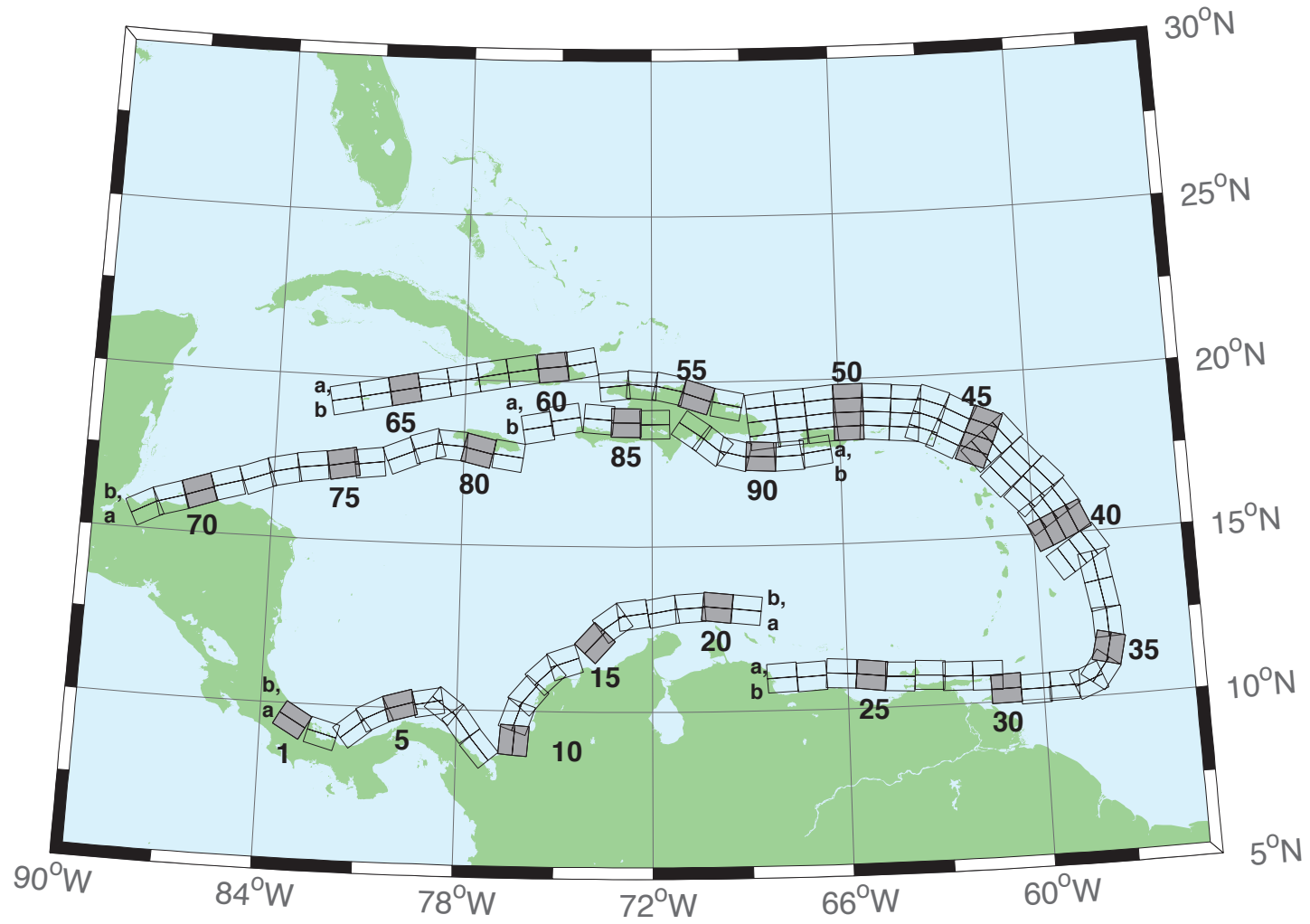


Figure B1: Atlantic Source Zone unit sources.

Table B1: Earthquake parameters for Atlantic Source Zone unit sources.

Segment	Description	Longitude(°E)	Latitude(°N)	Strike(°)	Dip(°)	Depth (km)
atsz-1a	Atlantic Source Zone	-83.2020	9.1449	120	27.5	28.09
atsz-1b	Atlantic Source Zone	-83.0000	9.4899	120	27.5	5
atsz-2a	Atlantic Source Zone	-82.1932	8.7408	105.1	27.5	28.09
atsz-2b	Atlantic Source Zone	-82.0880	9.1254	105.1	27.5	5
atsz-3a	Atlantic Source Zone	-80.9172	9.0103	51.31	30	30
atsz-3b	Atlantic Source Zone	-81.1636	9.3139	51.31	30	5
atsz-4a	Atlantic Source Zone	-80.3265	9.4308	63.49	30	30
atsz-4b	Atlantic Source Zone	-80.5027	9.7789	63.49	30	5
atsz-5a	Atlantic Source Zone	-79.6247	9.6961	74.44	30	30
atsz-5b	Atlantic Source Zone	-79.7307	10.0708	74.44	30	5
atsz-6a	Atlantic Source Zone	-78.8069	9.8083	79.71	30	30
atsz-6b	Atlantic Source Zone	-78.8775	10.1910	79.71	30	5
atsz-7a	Atlantic Source Zone	-78.6237	9.7963	127.2	30	30
atsz-7b	Atlantic Source Zone	-78.3845	10.1059	127.2	30	5
atsz-8a	Atlantic Source Zone	-78.1693	9.3544	143.8	30	30
atsz-8b	Atlantic Source Zone	-77.8511	9.5844	143.8	30	5
atsz-9a	Atlantic Source Zone	-77.5913	8.5989	139.9	30	30
atsz-9b	Atlantic Source Zone	-77.2900	8.8493	139.9	30	5
atsz-10a	Atlantic Source Zone	-75.8109	9.0881	4.67	17	19.62
atsz-10b	Atlantic Source Zone	-76.2445	9.1231	4.67	17	5
atsz-11a	Atlantic Source Zone	-75.7406	9.6929	19.67	17	19.62
atsz-11b	Atlantic Source Zone	-76.1511	9.8375	19.67	17	5
atsz-12a	Atlantic Source Zone	-75.4763	10.2042	40.4	17	19.62
atsz-12b	Atlantic Source Zone	-75.8089	10.4826	40.4	17	5
atsz-13a	Atlantic Source Zone	-74.9914	10.7914	47.17	17	19.62
atsz-13b	Atlantic Source Zone	-75.2890	11.1064	47.17	17	5
atsz-14a	Atlantic Source Zone	-74.5666	11.0708	71.68	17	19.62
atsz-14b	Atlantic Source Zone	-74.7043	11.4786	71.68	17	5
atsz-15a	Atlantic Source Zone	-73.4576	11.8012	42.69	17	19.62
atsz-15b	Atlantic Source Zone	-73.7805	12.0924	42.69	17	5
atsz-16a	Atlantic Source Zone	-72.9788	12.3365	54.75	17	19.62
atsz-16b	Atlantic Source Zone	-73.2329	12.6873	54.75	17	5
atsz-17a	Atlantic Source Zone	-72.5454	12.5061	81.96	17	19.62
atsz-17b	Atlantic Source Zone	-72.6071	12.9314	81.96	17	5
atsz-18a	Atlantic Source Zone	-71.6045	12.6174	79.63	17	19.62
atsz-18b	Atlantic Source Zone	-71.6839	13.0399	79.63	17	5
atsz-19a	Atlantic Source Zone	-70.7970	12.7078	86.32	17	19.62
atsz-19b	Atlantic Source Zone	-70.8253	13.1364	86.32	17	5
atsz-20a	Atlantic Source Zone	-70.0246	12.7185	95.94	17	19.62
atsz-20b	Atlantic Source Zone	-69.9789	13.1457	95.94	17	5
atsz-21a	Atlantic Source Zone	-69.1244	12.6320	95.94	17	19.62
atsz-21b	Atlantic Source Zone	-69.0788	13.0592	95.94	17	5
atsz-22a	Atlantic Source Zone	-68.0338	11.4286	266.9	15	17.94
atsz-22b	Atlantic Source Zone	-68.0102	10.9954	266.9	15	5
atsz-23a	Atlantic Source Zone	-67.1246	11.4487	266.9	15	17.94
atsz-23b	Atlantic Source Zone	-67.1010	11.0155	266.9	15	5
atsz-24a	Atlantic Source Zone	-66.1656	11.5055	273.3	15	17.94
atsz-24b	Atlantic Source Zone	-66.1911	11.0724	273.3	15	5
atsz-25a	Atlantic Source Zone	-65.2126	11.4246	276.4	15	17.94
atsz-25b	Atlantic Source Zone	-65.2616	10.9934	276.4	15	5
atsz-26a	Atlantic Source Zone	-64.3641	11.3516	272.9	15	17.94
atsz-26b	Atlantic Source Zone	-64.3862	10.9183	272.9	15	5
atsz-27a	Atlantic Source Zone	-63.4472	11.3516	272.9	15	17.94
atsz-27b	Atlantic Source Zone	-63.4698	10.9183	272.9	15	5
atsz-28a	Atlantic Source Zone	-62.6104	11.2831	271.1	15	17.94
atsz-28b	Atlantic Source Zone	-62.6189	10.8493	271.1	15	5
atsz-29a	Atlantic Source Zone	-61.6826	11.2518	271.6	15	17.94
atsz-29b	Atlantic Source Zone	-61.6947	10.8181	271.6	15	5
atsz-30a	Atlantic Source Zone	-61.1569	10.8303	269	15	17.94
atsz-30b	Atlantic Source Zone	-61.1493	10.3965	269	15	5
atsz-31a	Atlantic Source Zone	-60.2529	10.7739	269	15	17.94
atsz-31b	Atlantic Source Zone	-60.2453	10.3401	269	15	5
atsz-32a	Atlantic Source Zone	-59.3510	10.8123	269	15	17.94

Continued on next page

Table B1 – continued from previous page

Segment	Description	Longitude(°E)	Latitude(°N)	Strike(°)	Dip(°)	Depth (km)
atsz-32b	Atlantic Source Zone	-59.3734	10.3785	269	15	5
atsz-33a	Atlantic Source Zone	-58.7592	10.8785	248.6	15	17.94
atsz-33b	Atlantic Source Zone	-58.5984	10.4745	248.6	15	5
atsz-34a	Atlantic Source Zone	-58.5699	11.0330	217.2	15	17.94
atsz-34b	Atlantic Source Zone	-58.2179	10.7710	217.2	15	5
atsz-35a	Atlantic Source Zone	-58.3549	11.5300	193.7	15	17.94
atsz-35b	Atlantic Source Zone	-57.9248	11.4274	193.7	15	5
atsz-36a	Atlantic Source Zone	-58.3432	12.1858	177.7	15	17.94
atsz-36b	Atlantic Source Zone	-57.8997	12.2036	177.7	15	5
atsz-37a	Atlantic Source Zone	-58.4490	12.9725	170.7	15	17.94
atsz-37b	Atlantic Source Zone	-58.0095	13.0424	170.7	15	5
atsz-38a	Atlantic Source Zone	-58.6079	13.8503	170.2	15	17.94
atsz-38b	Atlantic Source Zone	-58.1674	13.9240	170.2	15	5
atsz-39a	Atlantic Source Zone	-58.6667	14.3915	146.8	15	17.94
atsz-39b	Atlantic Source Zone	-58.2913	14.6287	146.8	15	5
atsz-39y	Atlantic Source Zone	-59.4168	13.9171	146.8	15	43.82
atsz-39z	Atlantic Source Zone	-59.0415	14.1543	146.8	15	30.88
atsz-40a	Atlantic Source Zone	-59.1899	15.2143	156.2	15	17.94
atsz-40b	Atlantic Source Zone	-58.7781	15.3892	156.2	15	5
atsz-40y	Atlantic Source Zone	-60.0131	14.8646	156.2	15	43.82
atsz-40z	Atlantic Source Zone	-59.6012	15.0395	156.2	15	30.88
atsz-41a	Atlantic Source Zone	-59.4723	15.7987	146.3	15	17.94
atsz-41b	Atlantic Source Zone	-59.0966	16.0392	146.3	15	5
atsz-41y	Atlantic Source Zone	-60.2229	15.3177	146.3	15	43.82
atsz-41z	Atlantic Source Zone	-59.8473	15.5582	146.3	15	30.88
atsz-42a	Atlantic Source Zone	-59.9029	16.4535	137	15	17.94
atsz-42b	Atlantic Source Zone	-59.5716	16.7494	137	15	5
atsz-42y	Atlantic Source Zone	-60.5645	15.8616	137	15	43.82
atsz-42z	Atlantic Source Zone	-60.2334	16.1575	137	15	30.88
atsz-43a	Atlantic Source Zone	-60.5996	17.0903	138.7	15	17.94
atsz-43b	Atlantic Source Zone	-60.2580	17.3766	138.7	15	5
atsz-43y	Atlantic Source Zone	-61.2818	16.5177	138.7	15	43.82
atsz-43z	Atlantic Source Zone	-60.9404	16.8040	138.7	15	30.88
atsz-44a	Atlantic Source Zone	-61.1559	17.8560	141.1	15	17.94
atsz-44b	Atlantic Source Zone	-60.8008	18.1286	141.1	15	5
atsz-44y	Atlantic Source Zone	-61.8651	17.3108	141.1	15	43.82
atsz-44z	Atlantic Source Zone	-61.5102	17.5834	141.1	15	30.88
atsz-45a	Atlantic Source Zone	-61.5491	18.0566	112.8	15	17.94
atsz-45b	Atlantic Source Zone	-61.3716	18.4564	112.8	15	5
atsz-45y	Atlantic Source Zone	-61.9037	17.2569	112.8	15	43.82
atsz-45z	Atlantic Source Zone	-61.7260	17.6567	112.8	15	30.88
atsz-46a	Atlantic Source Zone	-62.4217	18.4149	117.9	15	17.94
atsz-46b	Atlantic Source Zone	-62.2075	18.7985	117.9	15	5
atsz-46y	Atlantic Source Zone	-62.8493	17.6477	117.9	15	43.82
atsz-46z	Atlantic Source Zone	-62.6352	18.0313	117.9	15	30.88
atsz-47a	Atlantic Source Zone	-63.1649	18.7844	110.5	20	22.1
atsz-47b	Atlantic Source Zone	-63.0087	19.1798	110.5	20	5
atsz-47y	Atlantic Source Zone	-63.4770	17.9936	110.5	20	56.3
atsz-47z	Atlantic Source Zone	-63.3205	18.3890	110.5	20	39.2
atsz-48a	Atlantic Source Zone	-63.8800	18.8870	95.37	20	22.1
atsz-48b	Atlantic Source Zone	-63.8382	19.3072	95.37	20	5
atsz-48y	Atlantic Source Zone	-63.9643	18.0465	95.37	20	56.3
atsz-48z	Atlantic Source Zone	-63.9216	18.4667	95.37	20	39.2
atsz-49a	Atlantic Source Zone	-64.8153	18.9650	94.34	20	22.1
atsz-49b	Atlantic Source Zone	-64.7814	19.3859	94.34	20	5
atsz-49y	Atlantic Source Zone	-64.8840	18.1233	94.34	20	56.3
atsz-49z	Atlantic Source Zone	-64.8492	18.5442	94.34	20	39.2
atsz-50a	Atlantic Source Zone	-65.6921	18.9848	89.59	20	22.1
atsz-50b	Atlantic Source Zone	-65.6953	19.4069	89.59	20	5
atsz-50y	Atlantic Source Zone	-65.6874	18.1407	89.59	20	56.3
atsz-50z	Atlantic Source Zone	-65.6887	18.5628	89.59	20	39.2
atsz-51a	Atlantic Source Zone	-66.5742	18.9484	84.98	20	22.1
atsz-51b	Atlantic Source Zone	-66.6133	19.3688	84.98	20	5
atsz-51y	Atlantic Source Zone	-66.4977	18.1076	84.98	20	56.3

Continued on next page

Table B1 – continued from previous page

Segment	Description	Longitude(°E)	Latitude(°N)	Strike(°)	Dip(°)	Depth (km)
atsz-51z	Atlantic Source Zone	-66.5353	18.5280	84.98	20	39.2
atsz-52a	Atlantic Source Zone	-67.5412	18.8738	85.87	20	22.1
atsz-52b	Atlantic Source Zone	-67.5734	19.2948	85.87	20	5
atsz-52y	Atlantic Source Zone	-67.4781	18.0319	85.87	20	56.3
atsz-52z	Atlantic Source Zone	-67.5090	18.4529	85.87	20	39.2
atsz-53a	Atlantic Source Zone	-68.4547	18.7853	83.64	20	22.1
atsz-53b	Atlantic Source Zone	-68.5042	19.2048	83.64	20	5
atsz-53y	Atlantic Source Zone	-68.3575	17.9463	83.64	20	56.3
atsz-53z	Atlantic Source Zone	-68.4055	18.3658	83.64	20	39.2
atsz-54a	Atlantic Source Zone	-69.6740	18.8841	101.5	20	22.1
atsz-54b	Atlantic Source Zone	-69.5846	19.2976	101.5	20	5
atsz-55a	Atlantic Source Zone	-70.7045	19.1376	108.2	20	22.1
atsz-55b	Atlantic Source Zone	-70.5647	19.5386	108.2	20	5
atsz-56a	Atlantic Source Zone	-71.5368	19.3853	102.6	20	22.1
atsz-56b	Atlantic Source Zone	-71.4386	19.7971	102.6	20	5
atsz-57a	Atlantic Source Zone	-72.3535	19.4838	94.2	20	22.1
atsz-57b	Atlantic Source Zone	-72.3206	19.9047	94.2	20	5
atsz-58a	Atlantic Source Zone	-73.1580	19.4498	84.34	20	22.1
atsz-58b	Atlantic Source Zone	-73.2022	19.8698	84.34	20	5
atsz-59a	Atlantic Source Zone	-74.3567	20.9620	259.7	20	22.1
atsz-59b	Atlantic Source Zone	-74.2764	20.5467	259.7	20	5
atsz-60a	Atlantic Source Zone	-75.2386	20.8622	264.2	15	17.94
atsz-60b	Atlantic Source Zone	-75.1917	20.4306	264.2	15	5
atsz-61a	Atlantic Source Zone	-76.2383	20.7425	260.7	15	17.94
atsz-61b	Atlantic Source Zone	-76.1635	20.3144	260.7	15	5
atsz-62a	Atlantic Source Zone	-77.2021	20.5910	259.9	15	17.94
atsz-62b	Atlantic Source Zone	-77.1214	20.1638	259.9	15	5
atsz-63a	Atlantic Source Zone	-78.1540	20.4189	259	15	17.94
atsz-63b	Atlantic Source Zone	-78.0661	19.9930	259	15	5
atsz-64a	Atlantic Source Zone	-79.0959	20.2498	259.2	15	17.94
atsz-64b	Atlantic Source Zone	-79.0098	19.8236	259.2	15	5
atsz-65a	Atlantic Source Zone	-80.0393	20.0773	258.9	15	17.94
atsz-65b	Atlantic Source Zone	-79.9502	19.6516	258.9	15	5
atsz-66a	Atlantic Source Zone	-80.9675	19.8993	258.6	15	17.94
atsz-66b	Atlantic Source Zone	-80.8766	19.4740	258.6	15	5
atsz-67a	Atlantic Source Zone	-81.9065	19.7214	258.5	15	17.94
atsz-67b	Atlantic Source Zone	-81.8149	19.2962	258.5	15	5
atsz-68a	Atlantic Source Zone	-87.8003	15.2509	62.69	15	17.94
atsz-68b	Atlantic Source Zone	-88.0070	15.6364	62.69	15	5
atsz-69a	Atlantic Source Zone	-87.0824	15.5331	72.73	15	17.94
atsz-69b	Atlantic Source Zone	-87.2163	15.9474	72.73	15	5
atsz-70a	Atlantic Source Zone	-86.1622	15.8274	70.64	15	17.94
atsz-70b	Atlantic Source Zone	-86.3120	16.2367	70.64	15	5
atsz-71a	Atlantic Source Zone	-85.3117	16.1052	73.7	15	17.94
atsz-71b	Atlantic Source Zone	-85.4387	16.5216	73.7	15	5
atsz-72a	Atlantic Source Zone	-84.3470	16.3820	69.66	15	17.94
atsz-72b	Atlantic Source Zone	-84.5045	16.7888	69.66	15	5
atsz-73a	Atlantic Source Zone	-83.5657	16.6196	77.36	15	17.94
atsz-73b	Atlantic Source Zone	-83.6650	17.0429	77.36	15	5
atsz-74a	Atlantic Source Zone	-82.7104	16.7695	82.35	15	17.94
atsz-74b	Atlantic Source Zone	-82.7709	17.1995	82.35	15	5
atsz-75a	Atlantic Source Zone	-81.7297	16.9003	79.86	15	17.94
atsz-75b	Atlantic Source Zone	-81.8097	17.3274	79.86	15	5
atsz-76a	Atlantic Source Zone	-80.9196	16.9495	82.95	15	17.94
atsz-76b	Atlantic Source Zone	-80.9754	17.3801	82.95	15	5
atsz-77a	Atlantic Source Zone	-79.8086	17.2357	67.95	15	17.94
atsz-77b	Atlantic Source Zone	-79.9795	17.6378	67.95	15	5
atsz-78a	Atlantic Source Zone	-79.0245	17.5415	73.61	15	17.94
atsz-78b	Atlantic Source Zone	-79.1532	17.9577	73.61	15	5
atsz-79a	Atlantic Source Zone	-78.4122	17.5689	94.07	15	17.94
atsz-79b	Atlantic Source Zone	-78.3798	18.0017	94.07	15	5
atsz-80a	Atlantic Source Zone	-77.6403	17.4391	103.3	15	17.94
atsz-80b	Atlantic Source Zone	-77.5352	17.8613	103.3	15	5
atsz-81a	Atlantic Source Zone	-76.6376	17.2984	98.21	15	17.94

Continued on next page

**Table B1 – continued from previous page**

Segment	Description	Longitude(°E)	Latitude(°N)	Strike(°)	Dip(°)	Depth (km)
atsz-81b	Atlantic Source Zone	-76.5726	17.7278	98.21	15	5
atsz-82a	Atlantic Source Zone	-75.7299	19.0217	260.1	15	17.94
atsz-82b	Atlantic Source Zone	-75.6516	18.5942	260.1	15	5
atsz-83a	Atlantic Source Zone	-74.8351	19.2911	260.8	15	17.94
atsz-83b	Atlantic Source Zone	-74.7621	18.8628	260.8	15	5
atsz-84a	Atlantic Source Zone	-73.6639	19.2991	274.8	15	17.94
atsz-84b	Atlantic Source Zone	-73.7026	18.8668	274.8	15	5
atsz-85a	Atlantic Source Zone	-72.8198	19.2019	270.6	15	17.94
atsz-85b	Atlantic Source Zone	-72.8246	18.7681	270.6	15	5
atsz-86a	Atlantic Source Zone	-71.9143	19.1477	269.1	15	17.94
atsz-86b	Atlantic Source Zone	-71.9068	18.7139	269.1	15	5
atsz-87a	Atlantic Source Zone	-70.4738	18.8821	304.5	15	17.94
atsz-87b	Atlantic Source Zone	-70.7329	18.5245	304.5	15	5
atsz-88a	Atlantic Source Zone	-69.7710	18.3902	308.9	15	17.94
atsz-88b	Atlantic Source Zone	-70.0547	18.0504	308.4	15	5
atsz-89a	Atlantic Source Zone	-69.2635	18.2099	283.9	15	17.94
atsz-89b	Atlantic Source Zone	-69.3728	17.7887	283.9	15	5
atsz-90a	Atlantic Source Zone	-68.5059	18.1443	272.9	15	17.94
atsz-90b	Atlantic Source Zone	-68.5284	17.7110	272.9	15	5
atsz-91a	Atlantic Source Zone	-67.6428	18.1438	267.8	15	17.94
atsz-91b	Atlantic Source Zone	-67.6256	17.7103	267.8	15	5
atsz-92a	Atlantic Source Zone	-66.8261	18.2536	262	15	17.94
atsz-92b	Atlantic Source Zone	-66.7627	17.8240	262	15	5

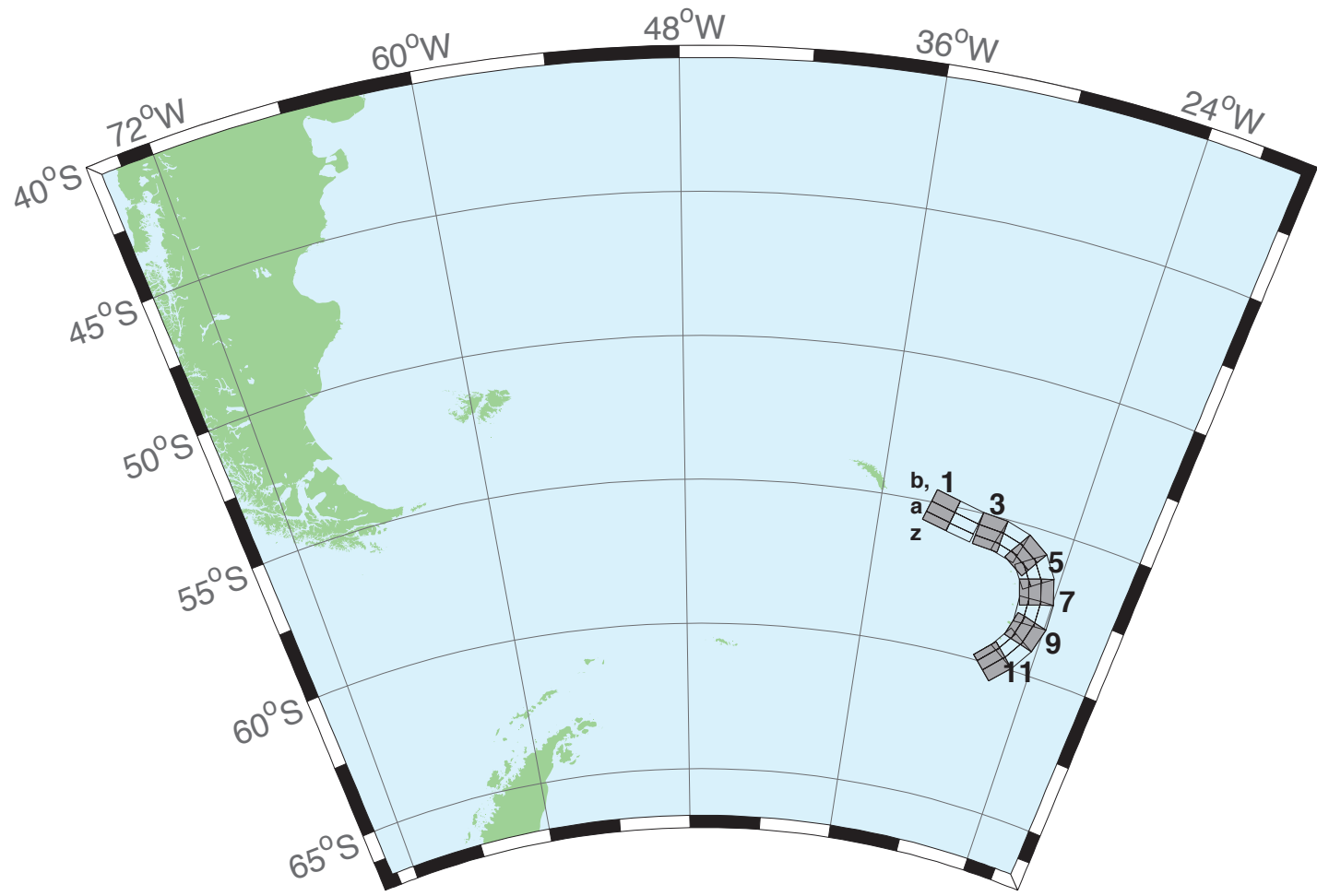


Figure B2: South Sandwich Islands Subduction Zone.

Table B2: Earthquake parameters for South Sandwich Islands Subduction Zone unit sources.

Segment	Description	Longitude(°E)	Latitude(°N)	Strike(°)	Dip(°)	Depth (km)
sssz-1a	South Sandwich Islands Subduction Zone	-32.3713	-55.4655	104.7	28.53	17.51
sssz-1b	South Sandwich Islands Subduction Zone	-32.1953	-55.0832	104.7	9.957	8.866
sssz-1z	South Sandwich Islands Subduction Zone	-32.5091	-55.7624	104.7	46.99	41.39
sssz-2a	South Sandwich Islands Subduction Zone	-30.8028	-55.6842	102.4	28.53	17.51
sssz-2b	South Sandwich Islands Subduction Zone	-30.6524	-55.2982	102.4	9.957	8.866
sssz-2z	South Sandwich Islands Subduction Zone	-30.9206	-55.9839	102.4	46.99	41.39
sssz-3a	South Sandwich Islands Subduction Zone	-29.0824	-55.8403	95.53	28.53	17.51
sssz-3b	South Sandwich Islands Subduction Zone	-29.0149	-55.4468	95.53	9.957	8.866
sssz-3z	South Sandwich Islands Subduction Zone	-29.1353	-56.1458	95.53	46.99	41.39
sssz-4a	South Sandwich Islands Subduction Zone	-27.8128	-55.9796	106.1	28.53	17.51
sssz-4b	South Sandwich Islands Subduction Zone	-27.6174	-55.5999	106.1	9.957	8.866
sssz-4z	South Sandwich Islands Subduction Zone	-27.9659	-56.2744	106.1	46.99	41.39
sssz-5a	South Sandwich Islands Subduction Zone	-26.7928	-56.2481	123.1	28.53	17.51
sssz-5b	South Sandwich Islands Subduction Zone	-26.4059	-55.9170	123.1	9.957	8.866
sssz-5z	South Sandwich Islands Subduction Zone	-27.0955	-56.5052	123.1	46.99	41.39
sssz-6a	South Sandwich Islands Subduction Zone	-26.1317	-56.6466	145.6	23.28	16.11
sssz-6b	South Sandwich Islands Subduction Zone	-25.5131	-56.4133	145.6	9.09	8.228
sssz-6z	South Sandwich Islands Subduction Zone	-26.5920	-56.8194	145.6	47.15	35.87
sssz-7a	South Sandwich Islands Subduction Zone	-25.6787	-57.2162	162.9	21.21	14.23
sssz-7b	South Sandwich Islands Subduction Zone	-24.9394	-57.0932	162.9	7.596	7.626
sssz-7z	South Sandwich Islands Subduction Zone	-26.2493	-57.3109	162.9	44.16	32.32
sssz-8a	South Sandwich Islands Subduction Zone	-25.5161	-57.8712	178.2	20.33	15.91
sssz-8b	South Sandwich Islands Subduction Zone	-24.7233	-57.8580	178.2	8.449	8.562
sssz-8z	South Sandwich Islands Subduction Zone	-26.1280	-57.8813	178.2	43.65	33.28
sssz-9a	South Sandwich Islands Subduction Zone	-25.6657	-58.5053	195.4	25.76	15.71
sssz-9b	South Sandwich Islands Subduction Zone	-24.9168	-58.6127	195.4	8.254	8.537
sssz-9z	South Sandwich Islands Subduction Zone	-26.1799	-58.4313	195.4	51.69	37.44
sssz-10a	South Sandwich Islands Subduction Zone	-26.1563	-59.1048	212.5	32.82	15.65
sssz-10b	South Sandwich Islands Subduction Zone	-25.5335	-59.3080	212.5	10.45	6.581
sssz-10z	South Sandwich Islands Subduction Zone	-26.5817	-58.9653	212.5	54.77	42.75
sssz-11a	South Sandwich Islands Subduction Zone	-27.0794	-59.6799	224.2	33.67	15.75
sssz-11b	South Sandwich Islands Subduction Zone	-26.5460	-59.9412	224.2	11.32	5.927
sssz-11z	South Sandwich Islands Subduction Zone	-27.4245	-59.5098	224.2	57.19	43.46

## C Forecast Model Testing

Authors: Lindsey Wright and Hongqiang Zhou

### C.1 Purpose

Forecast models are tested with synthetic tsunami events covering a range of tsunami source locations. Testing is also done with selected historical tsunami events when available.

The purpose of forecast model testing is three-fold. The first objective is to assure that the results obtained with NOAA's tsunami forecast system, which has been released to the Tsunami Warning Centers for operational use, are identical to those obtained by the researcher during the development of the forecast model. The second objective is to test the forecast model for consistency, accuracy, time efficiency, and quality of results over a range of possible tsunami locations and magnitudes. The third objective is to identify bugs and issues in need of resolution by the researcher who developed the forecast model or by the forecast software development team before the next version release to NOAA's two Tsunami Warning Centers.

Local hardware and software applications, and tools familiar to the researcher(s), are used to run the MOST model during the forecast model development. The test results presented in this report lend confidence that the model performs as developed and produces the same results when initiated within the forecast application in an operational setting as those produced by the researcher during the forecast model development. The test results assure those who rely on the Morehead City tsunami forecast model that consistent results are produced irrespective of system.

### C.2 Testing procedure

The general procedure for forecast model testing is to run a set of synthetic tsunami scenarios through the forecast system application and compare the results with those obtained by the researcher during the forecast model development and presented in the Tsunami Forecast Model Report. Specific steps taken to test the model include:

1. Identification of testing scenarios, including the standard set of synthetic events and customized synthetic scenarios that may have been used by the researcher(s) in developing the forecast model.
2. Creation of new events to represent customized synthetic scenarios used by the researcher(s) in developing the forecast model, if any.
3. Submission of test model runs with the forecast system, and export of the results from A, B, and C grids, along with time series.
4. Recording applicable metadata, including the specific version of the forecast system used for testing.
5. Examination of forecast model results from the forecast system for instabilities in both time series and plot results.

6. Comparison of forecast model results obtained through the forecast system with those obtained during the forecast model development.
7. Summarization of results with specific mention of quality, consistency, and time efficiency.
8. Reporting of issues identified to modeler and forecast software development team.
9. Retesting the forecast models in the forecast system when reported issues have been addressed or explained.

Synthetic model runs were tested on a DELL PowerEdge R510 computer equipped with two Xeon E5670 processors at 2.93 Ghz, each with 12 MBytes of cache and 32 GB memory. The processors are hex core and support hyper threading, resulting in the computer performing as a 24 processor core machine. Additionally, the testing computer supports 10 Gigabit Ethernet for fast network connections. This computer configuration is similar or the same as the configurations of the computers installed at the Tsunami Warning Centers so the compute times should only vary slightly.

### **C.3 Results**

The Morehead City forecast model was tested with SIFT version 3.2 for three synthetic scenarios. Test results from the forecast system and comparisons with the results obtained during the forecast model development are shown numerically in Table C1 and graphically in Figures C1 to C3. The results show that the minimum and maximum amplitudes and time series obtained from the forecast system agree with those obtained during the forecast model development, and that the forecast model is stable and robust, with consistent and high-quality results across geographically distributed tsunami sources. The model run time (wall-clock time) was 22.4 min for 12 hr of simulation time, and 7.4 min for 4.0 hr. This is within the 10 min run time for 4 hr of simulation and satisfies run time requirements.

Amplitudes of less than 75 cm were observed for all cases tested. The largest modeled height was 73 cm from the Atlantic (ATSZ 48-57) source zone. The smallest signal of 13 cm was recorded from the far-field South Sandwich (SSSZ 1-10) source zone. The comparisons between the development cases and the forecast system output were consistent in shape and amplitude for all three cases. The Morehead City reference point used for the forecast model development is the same as what is currently deployed in the forecast system, so the results can be considered valid for the three cases studied.

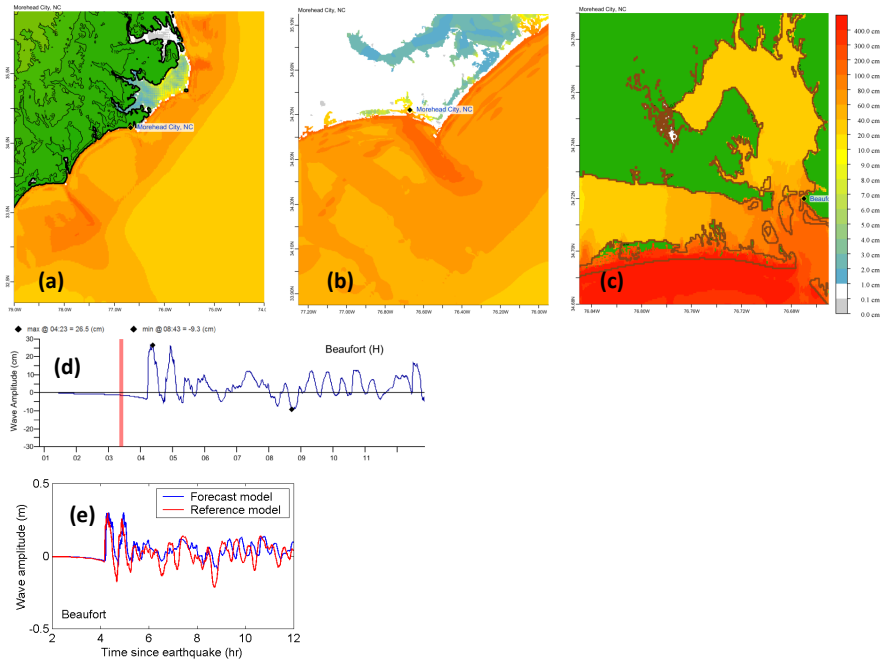


Figure C1: Response of the Morehead City forecast model to synthetic scenario ATSZ 38-47 ( $\alpha=25$ ). Maximum sea surface elevation for (a) A grid, (b) B grid, and (c) C grid. Sea surface elevation time series at the C-grid warning point (d). The lower time series plot is the result obtained during model development and is shown for comparison with test results.

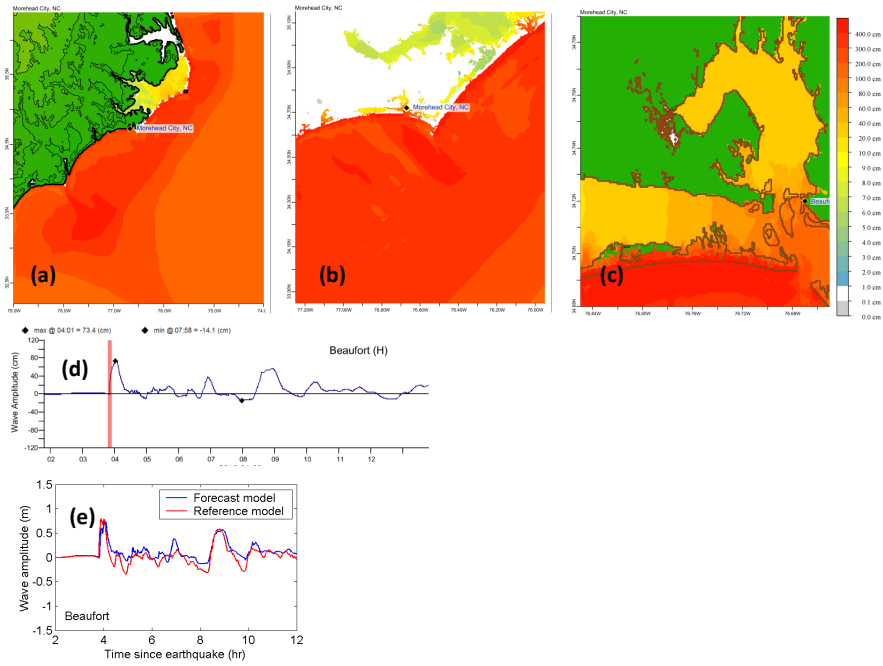


Figure C2: Response of the Morehead City forecast model to synthetic scenario ATSZ 48-57 ( $\alpha=25$ ). Maximum sea surface elevation for (a) A grid, (b) B grid, and (c) C-grid. Sea surface elevation time series at the C-grid warning point (d). The lower time series plot is the result obtained during model development and is shown for comparison with test results.

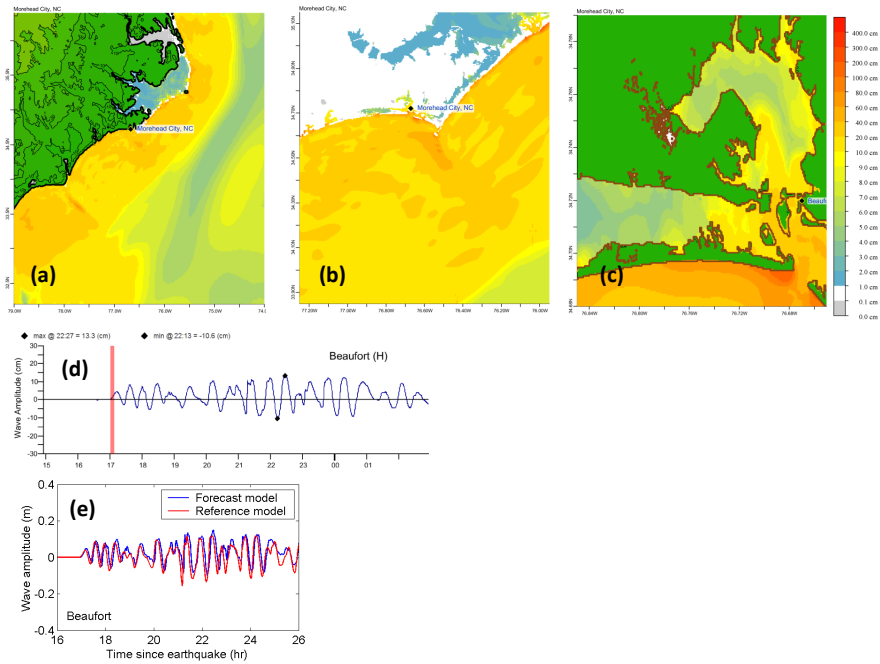


Figure C3: Response of the Morehead City forecast model to synthetic scenario SSSZ 1-10 ( $\alpha=25$ ). Maximum sea surface elevation for (a) A grid, (b) B grid, and (c) C grid. Sea surface elevation time series at the C-grid warning point (d). The lower time series plot is the result obtained during model development and is shown for comparison with test results.

Table C1: Table of maximum and minimum amplitudes (cm) at the Morehead City warning point for synthetic and historical events tested using SIFT 3.2 and obtained during development.

Scenario Name	Source Zone	Tsunami Source	$\alpha$ [m]	SIFT Max (cm)	Development Max (cm)	SIFT Min (cm)	Development Min (cm)
<b>Mega-tsunami Scenarios</b>							
ATSZ 38-47	Atlantic	A38-A47, B38-B47	25	26.5	30.0	-9.3	-8.6
ATSZ 48-57	Atlantic	A34-A57, B48-B57	25	73.4	74.0	-14.1	-13.1
SSSZ 1-10	South Sandwich Islands	A1-A10, B1-B10	25	13.3	15.0	-10.6	-9.7